UNIMORE
UNIVERSITÀ DEGLI STUDI DI MODENA E REGGIO EMILIA

DIPARTIMENTO DI MEDICINA E CHIRURGIA
PhD Course in Clinical and Experimental Medicine (CEM)-Medicina Clinica e Sperimentale
Ciclo XXXVIII

CLINICAL UTILITY OF IMAGING IN GIANT CELL ARTERITIS

TUTOR: ***Chiar.mo Prof.*** **CARLO SALVARANI**
CO-TUTOR: ***Chiar.mo Prof.*** **FRANCESCO MURATORE**

Direttore:
Chiar.mo Prof. **Marco Vinceti**

PhD Candidate:
Dr. CHIARA MARVISI

Anno Accademico 2024-2025

TABLE OF CONTENTS

ABSTRACT

Background Giant Cell Arteritis (GCA) encompasses a spectrum of phenotypes, ranging from cranial involvement (cranial-GCA) to large-vessel involvement (LV-GCA), with frequent overlapping manifestations. GCA is an important cause of non-infectious aortitis with potential for severe long-term complications such as aneurysm formation and dissection. Imaging modalities, particularly 18F-fluorodeoxyglucose positron emission tomography/computed tomography (18F-FDG PET/CT), are essential for diagnosis and monitoring, as they enable assessment of vascular inflammation and therapeutic response.

Visual assessment of PET scans employs a 4-point scoring system comparing arterial FDG uptake to hepatic activity. While practical, this approach is inherently subjective. Semi-quantitative techniques, including standardized uptake value (SUV)-based target-to-background ratios (TBR), offer enhanced reproducibility but are often time-consuming and may not accurately reflect the total inflammatory burden. Composite scoring systems such as PET Vascular Activity Score (PETVAS) or Total Vascular Score (TVS) provide semi-quantitative insights but can encounter limitations like ceiling effects or underestimation in segmental disease. Quantitative parameters, including total inflammatory vascular volume (TIVV) and total inflammatory glycolysis volume (TIGV), have been proposed to furnish a more comprehensive evaluation of disease activity.

This study aimed to:

1. Characterize baseline aortic involvement, estimate rate of aortic growth, and identify predictors of aneurysm development within a retrospective cohort.

2. Assess the utility of TIVV and TIGV in evaluating disease activity and predicting relapse or aortic dilatation in a prospective cohort.

Patients and Methods The project is divided into two parts, each using different cohorts to explore the two aims.

For the first aim, data were obtained from a retrospective cohort including patients diagnosed with GCA at two European referral centers. Aortic imaging was obtained via PET/CT, computed tomography angiography (CTA), and magnetic resonance angiography (MRA).

For the second aim, PET/CT scans conducted prospectively in the TOPAZIO study were included. PET/CT scans were re-analyzed through both visual and quantitative methods. TIVV and TIGV were calculated using automated algorithms.

Results The retrospective cohort comprised 157 patients. Baseline aortitis was identified in 60.4% of patients, with 19.6% presenting with aneurysms. The baseline aortic diameter was the strongest predictor of the aortic growth rate and aneurysm development. Although not significant the presence of aortitis was associated with aneurysm development primarily in patients receiving glucocorticoids (HRadj=3.2, 95% CI 0.65-15.7), suggesting the possibility of undertreatment or steroid-resistant disease.

The prospective cohort included 18 patients, with analysis of 61 PET/CT scans. TIVV and TIGV demonstrated strong associations with active disease (odds ratios: 4.74 [95% CI 1.23-18.2] and 5.45 [95% CI 1.36-21.8], respectively), as well as with relapse and aortic dilatation (hazard ratios: 2.50 [95% CI 1.07-5.84] and 2.23 [(95% CI 1.04-4.82], respectively). These volumetric parameters outperformed conventional PET metrics such as PETVAS and TVS. **Conclusion** Baseline aortic diameter is a significant predictor of subsequent aortic complications, emphasizing the importance of early imaging assessment.

TIVV and TIGV provide superior assessment of vascular inflammation and prognosis in LV-GCA compared to PET imaging parameters.

1. INTRODUCTION

Vasculitides are a heterogeneous group of diseases characterized by inflammation of the vessel wall. They are classified by the vessel caliber into large-vessel vasculitis (LVV), involving the aorta and its major branches; medium-vessel vasculitis (MVV), involving arterioles and venules; and small-vessel vasculitis (SVV), involving capillaries (1).

Giant Cell Arteritis (GCA) is classified with Takayasu's arteritis as a large-vessel vasculitis (1,2). Although initially described as temporal arteritis because of granulomatous inflammation in temporal artery biopsy (TAB) specimens, subsequent autopsy studies and rapid advances in vascular imaging beginning in the early twenty-first century have demonstrated arteritis and vessel wall inflammation in large vessels (3–6).

It is now recognized that GCA encompasses a broad phenotypic spectrum of medium- and large-artery inflammation. Nomenclature has evolved to reflect this, with terms such as large-vessel GCA (LV-GCA), cranial GCA (C-GCA), and LV-GCA with cranial involvement, depending on the site of inflammation (7).

1.1. Epidemiology

GCA is the most common primary vasculitis worldwide, although precise incidence estimates vary depending on the case definition criteria used, which are based on histological criteria (TAB), diagnostic coding, or classification criteria (8).

GCA occurs almost exclusively in patients aged >50 years, and the incidence increases with age, peaking in the eighth decade of life, with a 40-fold increase in disease risk compared with those aged 50–59 years (8–10). By contrast, patients with LV-GCA tend to be younger at onset. Women are more commonly affected than men, at a ratio of around 3:1 (10).

Both incidence and prevalence trends show a marked north–south gradient. GCA is reported to affect <10 cases per 100,000 persons aged 50 years or older in Mediterranean populations, whereas prevalence is particularly high among those of Scandinavian ancestry (8).

1.2. Pathogenesis

The pathogenesis of GCA is not fully understood, but several triggers have been proposed. Geographic and ethnic variations in GCA incidence suggest a substantial genetic contribution to disease etiology. In 2017, the first large genome-wide association study (GWAS) in GCA, including >2,000 individuals of European ancestry, confirmed a strong HLA class II association (11). This association is consistent with an antigen-driven immune response in pathogenesis and the predominance of CD4+ T cells within inflammatory lesions (12). The GWAS also identified risk polymorphisms in genes encoding plasminogen (PLG) and an isoform of the α-subunit of collagen prolyl 4-hydroxylase (P4HA2), which is essential for collagen biosynthesis, consistent with alterations in vascular remodeling (11).

Seasonal variation in GCA has suggested a potential role for microbial pathogens. Small epidemiological, clinical, and molecular studies have described potential links between GCA incidence and varicella zoster virus, Chlamydia pneumoniae, Mycoplasma spp., and parvovirus B19 (13–15). However, because elderly hosts commonly encounter multiple infections and microbial products may deposit in tissues, these findings do not prove causality for large-vessel inflammation, and there is no consistent evidence that any particular microorganism acts as a trigger for GCA.

The most interesting trigger is immunosenescence. Indeed, aging might be a contributing factor, since the risk of GCA increases with age. Immunosenescence leads to a reduction in naïve T cells and regulatory T cells (Tregs), increased production of pro-inflammatory cytokines, and reduced cellular response to inflammatory signals. In addition, aging is associated with changes in the elasticity of

the vessel walls. These changes are due to various causes, such as a reduction in vascular smooth muscle cells, media degeneration, calcium deposition, and intimal thickening (16,17).

All these triggers are thought to initiate the pathogenic mechanism model, which comprises several steps beginning with loss of immune tolerance in the arterial wall.

First, loss of Treg cells leads to failure to suppress pro-inflammatory T cells in lymph nodes (18). The age-associated decline of a specialized CD8+ Treg cell population is mechanistically linked to mis-trafficking of intracellular vesicles (17,19). Deficiencies in the PD1/PDL1 inhibitory pathway also contribute (20,21).

These deficiencies remove a natural brake on the adaptive immune system, rendering the artery vulnerable to autoimmune-driven inflammation. Both endothelial cells and vascular dendritic cells (DC) are naturally rich in PDL1 and function as protective shields against activated, injurious PD1-expressing T cells by binding PD1 and downregulating T cell activity.

Second, in GCA, circulating and vascular DCs lack PDL1 expression, leaving activated pro-inflammatory T cells unopposed. This results in enhanced vascular inflammation, increased production of the T cell cytokines interferon (IFN)γ, interleukin (IL)-17, and IL-21, excessive macrophage activation, and accelerated intimal hyperplasia (20–22).

The third mechanism is endothelial barrier leakiness, which normally prevents the migration of circulating cells into the vessel wall. In GCA, circulating monocytes produce excess matrix metalloproteases (MMPs), degrade the subendothelial basal lamina, and thereby enable T cells, which are independently capable of producing MMP2 and MMP9, to infiltrate (23–26). Additionally, adventitial endothelial cells aberrantly express Jagged1, a ligand for the receptor Neurogenic locus notch homolog protein 1 (NOTCH1) and interact with circulating CD4+NOTCH1+ T cells, promoting their differentiation into tissue-invasive effector cells that produce IL-17 and IFNγ (23,27).

Finally, immature neutrophils enriched in the blood of patients with GCA are potent producers of reactive oxygen species, enabling them to breach the endothelial barrier (28).

Inflammation-dependent neovascularization permits additional leukocyte–endothelial cell interactions and the propagation of inflammation (29).

In the vessel wall, DCs are activated and maintain innate and adaptive processes (12). In parallel, infiltrating macrophages differentiate into multinucleated giant cells (30). This process may persist for years. Effector T cells show a functional bias toward T Helper (Th)1 and Th17 (31,32). The cytokines produced further recruit and activate macrophages, which become the most important source of cytokines such as IL-6, IL-12, IL-23, and IL-1; growth factors such as vascular endothelial growth factor (VEGF) and platelet-derived growth factor (PDGF); and MMPs such as MMP9, MMP7, and MMP2 (23,33). Notably, VEGF primes endothelial cells, promotes further T cell influx, and drives vascular remodeling, intimal thickening, and neovascularization (23,33).

Various mechanistic studies have focused on the signaling pathways implicated in this process. Data point to NOTCH, Janus kinase–signal transducer and activator of transcription (JAK–STAT), and mammalian target of rapamycin (mTOR) (34,35). Blocking NOTCH signaling downregulates both Th1 and Th17 (27). Transcriptomic analyses of arterial tissue have indicated a critical pro-inflammatory role for JAK–STAT signaling in GCA, and treatment of immunodeficient mice carrying engrafted, inflamed human arteries with small-molecule JAK–STAT inhibitors is highly effective (36). The last one (mTOR) polarizes T cells toward a pro-inflammatory, effector cell state and has been detected in the endothelium of the aortic wall and in Th1 and Th17 cells derived from inflammatory lesions (37,38).

These data are of utmost importance, as they enable the identification of promising therapeutic targets.

1.3. Clinical presentation

The initial clinical presentation of GCA is highly variable, ranging from inflammatory to ischemic symptoms. Generally, patients with c-GCA present with cranial symptoms (headache, scalp tenderness), ischemic symptoms (jaw or tongue claudication), and visual symptoms. The most important emergency in this setting is permanent visual loss, which in 10-15% of cases is preceded by amaurosis fugax. In 80% of cases, anterior ischemic optic neuropathy (AION) is the cause, followed by central retinal artery occlusion (5–15% of cases) and transient diplopia (≤10%) (7,39).

Patients with predominant LV involvement more often present with systemic symptoms (low-grade fever, anorexia, fatigue, weight loss). Ischemic symptoms, such as limb or abdominal claudication, may also be present. A previous or concomitant diagnosis of polymyalgia rheumatica (PMR) is present in up to 40% of patients with GCA and is more frequent in those with LV involvement (7). Aortic complications, including dilation, aneurysm formation, and dissection, are severe long-term sequelae of LV-GCA. Up to one-third of patients develop an aortic aneurysm within 10 years of diagnosis, a complication associated with increased morbidity and mortality (40,41).

However, GCA should be considered a spectrum of disease with varying presentations. Hence, some patients may present with a predominant form of c-GCA or LV-GCA, while others may have overlapping features of both.

1.4. Diagnosis

The diagnostic process relies on clinical examination, imaging, and biopsy. Currently, there are no diagnostic criteria for GCA, and initial investigations are influenced by the clinical presentation (42). In any case, clinical examination of patients with suspected GCA should include the temporal, carotid, subclavian, and axillary arteries. Physical findings include painful nodules along the

temporal artery, asymmetric pulses, and vascular bruits in the carotid, axillary, or subclavian arteries.

Laboratory tests may also be useful and include acute-phase reactants, such as C-reactive protein (CRP) and erythrocyte sedimentation rate (ESR), which are markers of systemic inflammation and are elevated in 80-90% of patients (43,44). Notably, vasculitis may be part of systemic diseases, such as IgG4-related disease, systemic lupus erythematosus, or ANCA-associated vasculitis (45–47). Hence, levels of anti-neutrophil cytoplasm antibodies (ANCA), anti-nuclear antibodies (ANA), IgG4, C3 and C4, rheumatoid factor (RF), and cryoglobulin are warranted.

Of note, the absence of these findings does not rule out GCA; in cases of clinical suspicion, imaging should be obtained.

1.4.1.Cranial GCA

In the c-GCA subset, given the risk of irreversible vision loss associated with diagnostic delay, fast-track referral pathways have been developed for patients with GCA and have been shown to improve clinical outcomes and reduce health care costs (48).

The utility of color duplex sonography (CDS) of the superficial temporal arteries in diagnosing GCA is well known (49). Specific features that increase the exam's sensitivity and specificity include the "halo sign," characterized by homogeneous, hypoechoic wall thickening in affected vessels and representing vessel wall inflammation, and the "compression sign," defined as the persistence of visible thickening of the inflamed vessel wall after compression of the vessel lumen with the CDS probe (50). CDS offers several advantages in the diagnostic work-up of GCA. It is a non-invasive, safe, easily accessible, and repeatable procedure that does not expose patients to radiation. In fast-track clinics, CDS facilitates early diagnosis of GCA and has significantly reduced the incidence of severe ischemic complications. However, interpreting CDS findings requires careful consideration of the

clinical context (51). The halo sign, although indicative of GCA, may also be present in conditions mimicking GCA, such as atherosclerosis. False negatives are relatively common and may result from several factors: CDS accuracy depends heavily on the operator's expertise, and sensitivity can vary across GCA subsets (52). Additionally, the halo sign in superficial temporal arteries decreases rapidly once glucocorticoids (GCs) are started and typically disappears within 2–10 weeks (49,53–55).

In all cases that remain doubtful despite CDS, when c-GCA is suspected, temporal artery biopsy (TAB) remains the gold standard (2,56–58). It is a relatively quick and low-risk procedure that requires only local anesthesia. Surgical complications are rare and may include facial nerve injury or scalp necrosis (59–61).

A positive TAB result is highly specific for diagnosing GCA, with specificity approaching 100% (2,58). However, false negatives can occur, and reported sensitivity varies widely, ranging from 39% to 95% (62).

Several factors can influence the sensitivity of TAB, including the quality of specimen collection, histological work-up, and the pathologist's expertise in diagnosing GCA (63,64).

Compared to CDS, TAB allows ruling out mimickers of GCA with greater confidence (51,63). Furthermore, histological changes in temporal arteries in GCA patients may persist for months after steroid initiation (30,65). This provides a wider window of opportunity for diagnosis, despite ongoing treatment.

1.4.2.Large Vessel GCA

Multiple imaging modalities are available to assess the extent and severity of LVV, including CDS, magnetic resonance angiography (MRA), computed tomography angiography (CTA), and 18F-fluorodeoxyglucose (FDG)-PET with CT (PET/CT). Each modality has advantages and disadvantages, and use is typically guided by the clinical scenario and local expertise. Imaging of the aorta and its

major branches is recommended for all patients, including those with a primarily cranial presentation, because great vessel involvement may influence treatment strategy and prognosis.

The only extracranial arteries accessible to CDS are the carotid, subclavian, and axillary arteries, which should always be evaluated in the assessment of GCA (48,66,67). However, aortic assessment remains elusive.

MRA and CTA are both useful for examining the morphological features of the vessels. Although MRA is less prone to inter-operator variability than CDS, it is more expensive and less widely available yet provides a thorough assessment of the vessel wall and can accurately identify luminal abnormalities.

CTA is quicker and more widely available than MRA, with a sensitivity of 73% and specificity of 78% for diagnosing LV-GCA (68). However, its ability to identify vessel wall oedema and inflammation is probably inferior to that of MRA (48).

18F-FDG-PET/CT provides a functional map of large-vessel inflammation. Contiguous, high-grade vascular FDG uptake involving multiple arterial territories is typical of active LV-GCA (69). FDG uptake in vasculitis can be evaluated using both visual/qualitative and semi-quantitative methods (70). Visual assessment typically uses a 4-point scale (0-3) to compare FDG uptake in the arterial wall to the liver background (71). Cumulative arterial territory scores, such as the PET Vasculitis Activity Score (PETVAS) and the Total Vascular Score (TVS), reflect disease burden (72,73). This visual grading is consistent and easy to apply in clinical practice, but it depends on the reader's experience and remains subjective. In contrast, semi-quantitative methods involve regions of interest (ROIs) on PET images to calculate standardized uptake values (SUV) (70). Target-to-background ratios (TBRs), obtained by comparing arterial tissue SUVs to reference tissues such as the liver or blood pool, are also used to quantify arterial FDG uptake (74). Although semi-quantitative approaches are inherently more reproducible than visual assessment, they are more time-consuming and labor-

intensive. The drawbacks of PET include limited access, high cost, and long procedure times. Additionally, vascular FDG uptake is rapidly attenuated following treatment initiation. A study examining the diagnostic accuracy of PET after the introduction of high-dose prednisolone in 24 patients with active LVV showed that the FDG signal was reduced after 3 days of treatment; although the signal at this time point was still diagnostic in 100% of patients, by 10 days this figure had fallen to 36% (75). PET also requires a second imaging modality to map the low-definition functional image. Traditionally, this has been CT, which enables collection of high-quality structural imaging data simultaneously with functional data, albeit at considerable radiation exposure (42). More recently, hybrid scanners combining PET with MRI have demonstrated promising results with a fraction of the radiation exposure of CT (76,77). Further studies will determine whether hybrid PET–MRI is a useful diagnostic tool in LVV. Additionally, advances in PET radiotracers may enable active vascular inflammation to be distinguished from other pathologies such as atherosclerosis (78–80). Radioligands with specific affinity for activated macrophages, such as 11C-(R)-PK11195, have shown promise in small studies demonstrating the ability to track inflammation and differentiate active LVV from inactive disease (81). PET may be particularly valuable in cases of diagnostic uncertainty, for example, to exclude occult malignancy, whether combined with CT or MR.

1.5. Treatment

The mainstay of treatment for GCA remains high-dose GCs (56). GCs provide rapid symptom relief and reduce the risk of vision loss in GCA. The optimal initial GC dose and route of administration have not been thoroughly investigated, but the usual dose is 40–60 mg of oral prednisolone or equivalent per day, as recommended by the European League against Rheumatism (EULAR) and American College of Rheumatology (ACR) guidelines (56,57). For more rapid, intensive effect,

patients with GCA-related sight-threatening symptoms may receive pulsed intravenous methylprednisolone.

Following EULAR guidelines, disease-modifying agents in patients with GCA are reserved for those with relapsing or refractory disease or for those at increased risk of GC-related adverse effects, such as hypertension, osteoporosis, diabetes, or glaucoma (56). The efficacy of the IL-6 receptor-blocking humanized monoclonal antibody tocilizumab was demonstrated in the phase III Giant Cell Arteritis Actemra (GiACTA) trial, which included both newly diagnosed and relapsing patients with GCA (82). Treatment with tocilizumab resulted in a significantly higher proportion of patients in sustained remission at week 52, a longer time to disease flare, lower cumulative GC doses, and improved quality of life compared with placebo. Weekly dosing provided better disease control than every-other-week dosing, particularly in relapsing and refractory cases (82). However, >40% of patients were unable to maintain disease remission despite adherence to recommended GC tapering, and extended follow-up data show that only 40% of initial responders maintain treatment-free disease remission after 3 years (83).

Thus, tocilizumab should be continued for longer than the 52 weeks initially assessed in the GiACTA trial, and other options might be needed.

Recently, a phase III randomized controlled trial demonstrated the efficacy and safety of upadacitinib (a selective JAK inhibitor that blocks signaling by several cytokines, including interleukin-6 and interferon-γ) in patients with newly diagnosed and relapsing GCA. At 15 mg, upadacitinib was superior to placebo in inducing sustained complete remission, reducing time to disease flare, lowering cumulative GC exposure, and improving patient-reported outcomes (84).

Once disease remission is achieved, GCs should be tapered, usually after 2-4 weeks. EULAR guidelines suggest a dose of 15–20 mg of prednisolone (or equivalent) per day after 2–3 months and ≤5 mg/day after 1 year (56).

Evidence suggests that more rapid tapering may be feasible in GCA. In the GiACTA trial, sustained prednisone-free remission at week 52 was achieved by 14% of patients enrolled in the placebo arm with a 26-week GC taper and 18% with a 52-week GC taper. 68% of patients in the 26-week and 49% in the 52-week regimen taper presented at least one relapse during the first year. No patients in the two placebo arms developed ischemic manifestations after GC initiation (82). However, in the 2-year extension, 71% of patients treated with only GCs relapsed (85). Hence, the EULAR recommends the use of the 26-week GC taper regimen only in combination with tocilizumab, not as initial monotherapy, in standard clinical practice (56).

By contrast, tocilizumab monotherapy is currently contraindicated. Two open-label studies have evaluated the efficacy and safety of one year of tocilizumab monotherapy, preceded by three courses of intravenous methylprednisolone (86,87). The first study included patients with c-GCA, and 1/18 developed AION (86). The second study included only patients with LV-GCA, but concerns arose regarding vascular damage. An increased ascending aortic diameter was observed in 4 patients before week 52 and in 1 patient at week 78. Aortic aneurysm surgical repair was required in 2 patients, 1 at week 44 and 1 after 134 weeks from tocilizumab withdrawal. Histology revealed active granulomatous aortitis (87). Thus, tocilizumab monotherapy cannot currently be recommended for remission induction.

1.6. Management of follow-up

According to the EULAR guidelines, remission in LVV is defined as the absence of clinical signs and symptoms attributable to LVV, the absence of vascular damage on CTA, and normalization of CRP and ESR (48,56). However, RCTs have used different definitions of remission. In the GiACTA trial, remission was defined as the absence of LVV-related signs and symptoms and normalization of CRP (82).

Generally, the evaluation of disease activity relies on clinical and laboratory assessments.

However, several drawbacks of these evaluations limit the physician's ability to accurately assess disease activity. Clinical symptoms may be nonspecific (such as fever, fatigue, weight loss) or not clearly related to active disease (such as limb claudication). CRP and ESR may be normal even during active disease, especially in patients treated with tocilizumab (82).

In this context, imaging is helpful and should be considered a biomarker of disease activity.

1.7. Rationale of the study

Currently, there is no available tool to assess disease activity. Although imaging can serve as a biomarker for disease activity, the EULAR guidelines only recommend repeating 18F-FDG PET/CT when a relapse is suspected. For long-term monitoring of vascular structural damage, MRA or CTA may be used, although the timing for these procedures is not specified (48).

This is a major unmet need: although vision loss occurs early in the disease course, often before or within the first days of GC initiation, aortic aneurysms may be present at diagnosis but are more often a late complication. In a cohort of 332 patients with GCA, 14% of those with LV-GCA at diagnosis had developed aortic aneurysms within 4 years, compared with 5% of those with C-GCA at the outset (7). Patients with GCA have a 3- to 17-fold increased risk of thoracic aortic aneurysms, and a meta-analysis of studies with systematic imaging reported a pooled prevalence of 15% (88–91). Furthermore, a retrospective study evaluated patients who underwent thoracic aortic surgery between January 1, 2000, and December 31, 2021, and assessed whether histopathological features of active aortitis were present. Of 49 patients with a prior diagnosis of GCA, 40 (82%) presented with active aortitis, and all were considered in clinical remission (92). Taken together, these findings indicate that more data are needed on the risk of developing aortic dilation, aneurysm, or dissection.

While 18F-FDG PET/CT is widely recognized as the preferred imaging method for diagnosis, its role in predicting relapse or vascular damage remains uncertain. A 2015 meta-analysis of 11 studies (four on GCA involving 57 patients and seven on Takayasu Arteritis involving 191 patients) reported pooled sensitivities of 90% and specificities of 98% for diagnosing GCA (93). However, different studies have not consistently shown a connection between baseline PET parameters, whether visual, semi-quantitative, or quantitative, and future relapses (94). Some research, however, indicates an association between PETVAS during clinical remission and subsequent flare-ups (73). This discrepancy might be because regional uptake from single lesions does not fully reflect the overall inflammatory burden (73,74,94,95). Therefore, there is a need for new, standardized imaging evaluation techniques that can better assess disease activity and predict future relapse or vascular damage.

1.8. Aims of the study

The aims of the present study were:

1) to describe baseline aortic involvement; estimate the rate of aortic growth over time; and identify predictors of aneurysm development and aortic enlargement in a retrospective cohort;
2) to investigate the role of two quantitative parameters, the total inflammatory vascular volume (TIVV) and the total inflammatory glycolysis volume (TIGV), in assessing disease activity, predicting relapses, and the onset or progression of aortic dilatation in a cohort of GCA patients enrolled in a prospective study,
3) to compare these novel quantitative parameters, TIVV and TIGV, with conventional PET parameters, including visual score, PETVAS, TVS, SUVmean, and SUVmax.

2. PATIENTS AND METHODS

2.1. Aortitis and predictors of aortic dilation

2.1.1.Study design and population

For the first aim, a retrospective cohort study was conducted using prospectively collected data from patients diagnosed with GCA between January 2009 and December 2023 at two European referral centers: the Azienda Unità Sanitaria Locale–IRCCS di Reggio Emilia (Italy) and the University Hospital of Würzburg (Germany). Patients were included if they met all the following criteria:

- Age >50 years at diagnosis
- GCA confirmed by temporal artery biopsy and/or imaging of cranial or large vessels
- Availability of baseline thoracic aortic imaging within 6 months of diagnosis
- At least one follow-up thoracic aortic imaging performed ≥6 months after baseline
- Fulfillment of the 2022 ACR EULAR classification criteria for GCA (2).

Medical records of the patients included were reviewed from the date of GCA diagnosis to the last available aortic imaging. Patients with at least 6 months of follow-up were included. Data were recorded using a standardized electronic data collection form. Abstracted data included demographics (age and sex at diagnosis), cardiovascular risk factors (smoking, hypertension, hypercholesterolemia, diabetes), clinical features (cranial symptoms: any of headache, scalp tenderness, temporal artery abnormalities on physical examination; visual symptoms: any of diplopia, amaurosis fugax, partial or complete visual loss; ischemic symptoms: any of jaw claudication, visual manifestations, stroke, transient ischemic attacks; systemic symptoms: any of weight loss of at least 4 kg, fever), laboratory findings (ESR, CRP) and histology findings, and medical treatment (initial GC doses, GC dose and duration at the time of first imaging).

Relapse was defined as the reappearance of symptoms of GCA and/or PMR requiring treatment escalation.

2.1.2. Imaging assessment

All imaging studies, regardless of the indication, were included and reviewed. Aortic imaging included CT/CTA, MRI/MRA, and FDG PET/CT. Evaluated aortic segments were the mid-ascending aorta, aortic arch, mid-descending thoracic aorta, and suprarenal abdominal aorta. All segments were assessed as normal or abnormal, with abnormalities including aortitis, dilation/aneurysm, or dissection.

PET/CT scans were independently evaluated by one nuclear medicine specialist per site using the visual 0-3 vascular-to-liver FDG uptake grading scale (71). Scans with grade 2 or 3 FDG uptake were classified as aortitis (70).

All morphological imaging (CT/CTA, MRI/MRA) was independently reviewed by two radiologists per site. Aortitis was defined as vessel wall thickening and/or edema, with or without contrast enhancement (48). For each segment, the aortic diameter was measured on images reconstructed in a plane orthogonal to the direction of blood flow. For PET/CT scans, the non-contrast-enhanced CT study was used.

Aortic dilation was defined as >40 mm for the mid-ascending aorta, ≥40 mm for the aortic arch and mid-descending thoracic aorta and ≥30 mm for the suprarenal abdominal aorta (96). For the mid-ascending aorta, we also referred to the American College of Cardiology/American Heart Association (ACC/AHA) definition, which considers an ascending aortic diameter ≥4.5 cm as aneurysmal, based on data showing a marked increase in the relative risk of dissection beyond this threshold (97).

The velocity in the growth of the aorta was assessed as the velocity in the dilation of the aortic area.

Aortic dissection was identified by the presence of an intimal flap.

Primary outcomes included:

- Aortic diameter and prevalent aortic aneurysm at baseline.

- Incident aneurysm and aortic growth during follow-up assessed by annualized area changes in mm2/year per segment.

2.1.3.Statistical analyses

Categorical variables were reported as proportions, and continuous variables were reported as mean (standard deviation, SD) or median (interquartile range: Q1–Q3), as appropriate.

Comparisons between patients with and without aortitis were performed using the χ^2 test or Fisher's exact test for categorical variables and the t-test or Mann-Whitney U test for continuous variables.

Analyses were performed at both the patient and aortic segment levels, where applicable (**Figure 1**). Segment-level predictors included the presence of aortitis in the individual aortic district and the corresponding baseline diameter. In segment-level analyses, we computed the variance of the estimates while accounting for the non-independence of observations. To account for the non-independence of observations from the same individual in segment-level analyses, we used the clustered variance-covariance estimator ("vce cluster" option), which computes robust standard errors by treating individuals as clusters.

Multivariable linear regression was used to identify predictors of baseline aortic diameter and aortic growth, whereas logistic regression was used to assess predictors of prevalent aneurysm. Cox proportional hazards models were used to evaluate factors associated with incident aneurysm formation. Aortic growth during follow-up was calculated as the change in aortic area from baseline to follow-up, divided by the time interval between the first and last imaging (expressed in mm^2/year). Aortic area at each location was calculated using the formula $\pi \times r^2$, where r = diameter/2.

In evaluating aortic growth, to reduce confounding from differential follow-up time, six months of follow-up were added to all patients. Additionally, one outlier with extreme, rapidly progressive aortic dilation was excluded to improve model robustness (**Figure 2**).

All regression models were adjusted for age and sex. Analyses were further stratified by GC treatment status at baseline imaging (yes vs. no). The presence of aortitis was also adjusted for study center (Reggio Emilia or Würzburg) and imaging modality (PET/CT or MRI).

Analyses were performed using STATA 18.0.

Figure 1. Synopsis of the planned and reported analyses. Columns represent the different outcomes of interest: aortic diameter, aneurysm, and rate of area increase. Rows indicate the analytical perspective, cross-sectional or prospective, and the statistical unit of analysis, either the patient or the aortic segment. For each row at the patient level, the first column lists the characteristics investigated as potential determinants. Analyses at the aortic segment level are further divided into overall and segment-type–specific analyses. Gray cells denote analyses that are either not meaningful (e.g., cross-sectional analysis of velocity) or not feasible due to insufficient statistical power. Note that the aneurysm outcome reflects prevalence in cross-sectional analyses and incidence in prospective analyses.

Figure 2. Expansion rate of aortic area over time

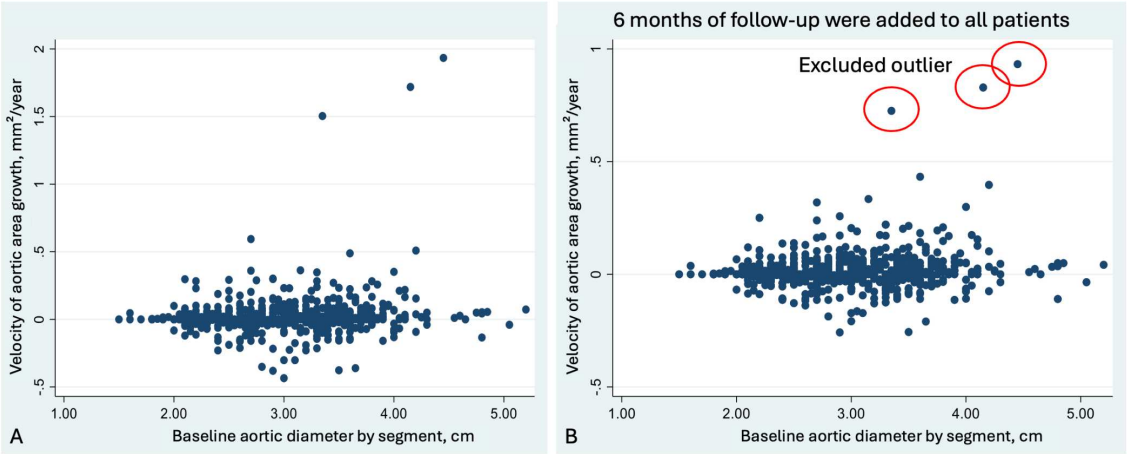

2.2. The role of TIVV and TIGV as diagnostic and prognostic biomarkers

2.2.1. Study design and population

For the second and third aims, data were obtained from the prospective cohort of patients enrolled in the study Treatment Of giant cell arteritis Patients with ultra-short glucocorticoids And TociliZumab: role of Imaging in a prospective Observational study (TOPAZIO) (87). This trial involved patients aged ≥50 years with a diagnosis of LV-GCA based on a PET/CT scan showing an FDG uptake ≥2 in at least one large artery, ESR >40 mm/h or CRP >10 mg/L, and symptoms of GCA or polymyalgia rheumatica. All patients were treated with three intravenous methylprednisolone boluses (500 mg/day) followed by weekly tocilizumab (162 mg) for 52 weeks. At week 52, relapse-free patients discontinued tocilizumab and entered a 26-week observational follow-up period (98). PET/CT scans were performed at baseline and at 24, 52, and 78 weeks (87,98).

A cross-sectional design was conducted to evaluate the diagnostic value of the PET parameters (active disease vs remission). A prospective cohort design was used to assess the prognostic value of the same parameters (relapse and/or aortic dilation vs non-relapse/aortic dilation). For the latter, since an active PET was an inclusion criterion of the observational trial TOPAZIO, the baseline scans were excluded (**Figure 3**).

Remission was defined according to the EULAR definition (56). Relapse was determined by the investigator and defined as one or more of the following: recurrence of signs or symptoms of GCA; CRP values greater than 10 mg/L, or ESR values greater than 40 mm/h, if considered by the investigator to be due to GCA; evidence of worsening vascular FDG uptake on PET/CT. The definition of relapse also included treatment restart with GC and/or tocilizumab. Non-response to treatment was defined as not achieving remission by week 16.

Aortic dilation was defined as previously described (96).

2.2.2. Imaging assessment

All PET/CT scans were retrospectively reviewed.

Visual assessment was performed by an experienced nuclear medicine physician who was aware of the order of the scans but not of the patients' clinical status. Visual assessment was rated on a 0-3 scale. Uptake was scored as '0' when there was no visible uptake, '1' when uptake was lower than the liver, '2' when it was equal to liver uptake, and '3' when it was significantly higher than liver uptake (71). Scans showing grades 2 and 3 were considered active (70). PETVAS and TVS were calculated by summing the visual uptake across 9 and 7 arterial territories, respectively (72,73).

TIVV was automatically calculated for all PET using the open-source Beth Israel PET/CT viewer plugin for FIJI (http://petctviewer.org). The reference value was the liver SUVmean measured within a 3 cm-diameter ROI in the right lobe. TIVV was defined using a vascular SUVmax threshold relative to liver SUVmean: G1 was < -10% liver SUVmean, G2 (grade 2) was the range from -10% to +10% liver SUVmean, and G3 (grade 3) was > 10% liver SUVmean. The following arterial segments were explored: the whole aorta (ascending aorta, aortic arch, descending thoracic aorta, and abdominal aorta), supraaortic arteries (innominate artery, subclavian arteries, common carotids), and common iliac arteries. TIVV was obtained by summing the inflammatory vascular volumes (IVV) of all vascular regions. Areas of increased physiological uptake, such as the brain, bladder, myocardium, or thymus, were manually excluded (**Figure 4**).

TIGV was defined mathematically as TIVV x SUVmean.

Grade 2 and 3 TIVV were calculated. Grade 1 was considered negative and excluded from calculation. For better comparison with Visual Score, PETVAS and TVS, SUVmean, TIVV, and TIGV included G2 and G3; SUVmean G3, TIVVG3, and TIGVG3 included only grade 3.

2.2.3.Statistical analyses

Categorical variables were reported as proportions, and continuous variables were reported as mean (SD) or median (Q1–Q3), as appropriate.

The diagnostic role of PET parameters in distinguishing active disease from remission, treated as a dichotomous outcome, was assessed using logistic regression. Models were not adjusted for age, as it was not associated with relapse (odds ratio [OR] 1.002, 95% CI 0.96-1.05, p-value 0.928), and adjustment did not change the OR estimates for the PET parameters. The variance of the ORs was computed using robust estimators that accounted for the non-independence of measures from the same patient. PET parameters were standardized to a mean of 0 and an SD of 1, and OR were calculated per one SD increase, except for the visual score, which is categorical. The analysis was performed on all 61 observations and, separately, on the 43 remaining observations after excluding baseline observations (**Figure 3a, Figure 3b**).

The prognostic role of PET parameters was examined using a Cox regression model adjusted for age. All PET parameters (except the visual score) were standardized, and hazard ratios (HR) were calculated per one SD increase. The outcome variable was disease relapse or aortic dilatation. Follow-up time began on the date of the baseline PET, with time to event as the time axis. All patients were followed until the last available visit, relapse, or aortic dilatation, whichever occurred first (**Figure 3c**). Nonresponders were excluded from the analysis.

Lastly, a Cox regression model was used to assess the prognostic role of early changes in PET parameters, i.e., from baseline to 24 weeks, in predicting disease relapse or aortic dilatation. In this analysis, follow-up time began at the midpoint between the baseline and 24-week PET scans, with time to event as the time axis. All patients were followed until the last available visit from the first PET, relapse, or aortic dilatation, whichever occurred first (**Figure 3d**).

In these analyses, because the sample was sized for a different primary endpoint, we did not use a p-value threshold to reject the null hypothesis. Confidence intervals should be interpreted as

measures of the precision of the point estimates for the OR and HR. P-values are reported as continuous values representing the probability of observing a given difference in odds or hazards under the null hypothesis of no difference.

Analyses were performed using STATA 18.0.

Figure 3. (a) Cross-sectional analysis. In this analysis, the outcome (active disease) and the PET parameters were assessed simultaneously at different time points: baseline, 24 weeks, 52 weeks and 76 weeks. The same patient can be included in the analysis more than once. (b) Cross-sectional analysis (excluding baseline measurements): in analysis, the outcome (active disease) and PET parameters were still considered at the same time. However, baseline measurements were excluded from the analysis. This exclusion removes the bias coming from PET positivity being a necessary inclusion criterion. Indeed, cases at baseline are, by definition, both active disease and PET-positive, thereby artificially inflating the association. (c) Longitudinal analysis (baseline PET parameters): in this longitudinal analysis, the association between baseline PET parameters and the outcome (disease relapse or aortic dilatation) was assessed over time. PET parameters were assessed at baseline, while the outcome was evaluated throughout the follow up period. Non-responders were excluded from the analysis. (d) Longitudinal analysis (change in PET parameters): this analysis assessed the association between the difference in PET values between baseline and week 24, and disease relapse or aortic dilatation over time. The exposure was assessed as the change in PET parameters (delta) between PET scan at baseline and at week 24. Non-responders were excluded from the analysis; relapses assessed at 24 weeks were included.

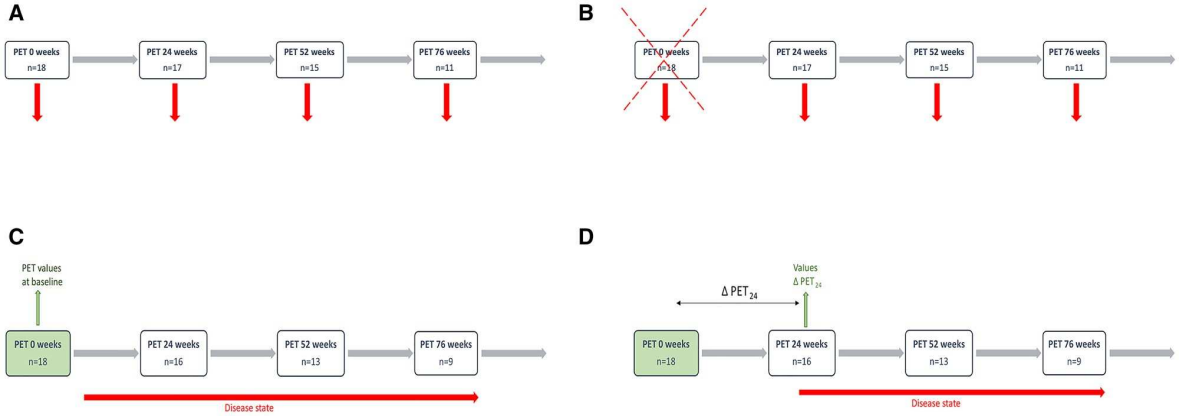

Figure 4. PET/CT images ((A) MIP anterior view. (B) coronal anterior view. (C) MIP lateral view. (D) coronal lateral view) showing intense 18F-FDG uptake along the walls of the large vessels, with uptake levels exceeding that of the liver. These regions were included in the TIVV calculation. MIP: maximum intensity projection; TIVV: total inflammatory vascular volume.

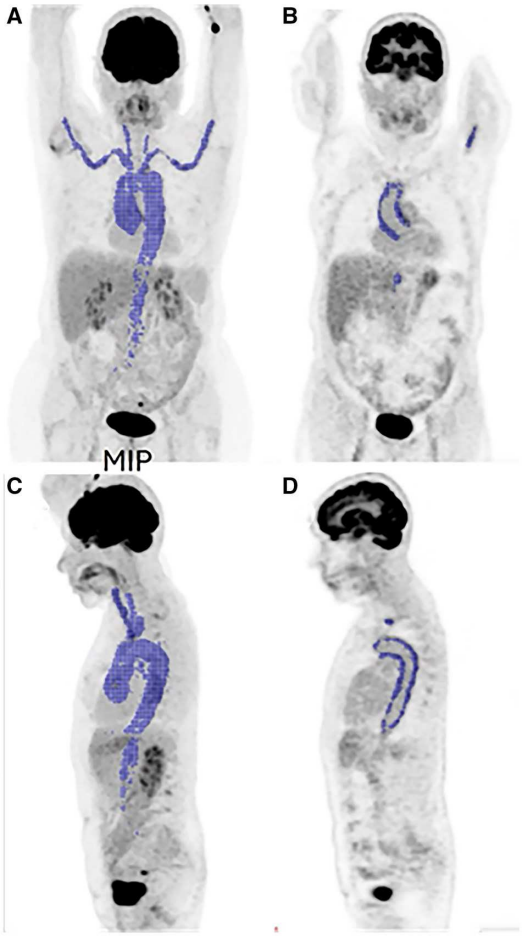

3. RESULTS

3.1. Aortitis and predictors of aortic dilation

3.1.1.Cohort description

A total of 157 patients were included (mean [S.D.] age 67.9 [9.1] years; 69.4% female). Demographic, clinical, and imaging characteristics of the study population are summarized in **Table 1**. Of the cohort, 41.4% were enrolled in Würzburg and 58.6% in Reggio Emilia. TAB was performed in 52 patients (33.1%), and it was positive in 34 cases (65.4%). At baseline, 43 patients (27.4%) underwent combined MRI/MRA, while 114 (72.6%) underwent PET/CT. No patient underwent baseline CT.

Aortitis was identified in 93/154 patients (60.4%) at baseline, detected in 32.6% of MRI/MRAs and 71.2% of PET/CT scans. Overall, aortitis was detected in 310/616 (50.3%) vascular segments evaluated: 77 mid-ascending aorta, 80 aortic arch, 81 mid-descending aorta, and 72 suprarenal aorta. Distribution of patients according to the time from diagnosis to imaging is reported in **Figure 5**. GC treatment was started before baseline imaging in 39.6% of patients, equally distributed between those with and without aortitis. Mean prednisone dose at the time of imaging was 16.8 mg/day, and median duration was 30 days. No patients were receiving tocilizumab at the time of baseline imaging. Compared with those without aortitis, patients with aortitis were younger (66.5 vs 69.7 years, $P = 0.028$), had a significantly lower prevalence of cranial (42.4% vs 65.0%, $P = 0.006$), visual (6.5% vs 28.3%, $P < 0.0001$), and ischemic symptoms (18.5% vs 41.7%, $P = 0.002$), were on a lower prednisone dose at first imaging (13.3 vs 20.3 mg/day, $P = 0.001$) and for a longer duration (40 vs 22 days, $P = 0.016$), and were more frequently enrolled at the Reggio Emilia center.

Table 1. Clinical and imaging characteristics of patients with and without aortitis

	Overall n 157	With Aortitis n 93	Without Aortitis n 61	p
Age (years), mean (SD)	67.9 (9.1)	66.5 (8.9)	69.7 (9.0)	0.028
Female	109 (69.4)	65 (69.9)	41 (67.2)	0.726
Hypercholesterolemia	56/156 (35.9)	28/92 (30.4)	26/61 (42.6)	0.122
Hypertension	99/156 (63.5)	58/92 (63)	41/61 (67.2)	0.597
Diabetes	19/155 (12.3)	11/92 (12)	8/60 (13.3)	0.802
Current smoker	37/155 (23.9)	23/92 (25)	14/60 (23.3)	0.815
Center				0.037
Würzburg	65 (41.4)	33 (50.8)	32 (49.2)	
Reggio Emilia	92 (58.6)	60/89 (67.4)	29/89 (32.6)	
Cranial symptoms	81/155 (52.3)	39/92 (42.4)	39/60 (65)	0.006
Visual symptoms	24/155 (15.5)	6/92 (6.5)	17/60 (28.3)	<0.0001
Ischemic symptoms	44/155 (28.4)	17/92 (18.5)	25/60 (41.7)	0.002
Systemic symptoms	91/155 (58.7)	57/92 (62)	33/60 (55)	0.394
PMR	43/155 (27.7)	26/92 (28.3)	17/60 (28.3)	0.992
TAB positive*	34/52 (65.4)	12/21 (57.1)	19/28 (67.9)	0.441
GCs at first imaging	59/149 (39.6)	30/87 (34.5)	29/59 (49.2)	0.076
Prednisone dose (mg/day), mean (SD)	16.8 (16.2)	13.3 (15.4)	20.3 (16.6)	0.001
Duration of GCs treatment (days), median (Q1, Q3)	30 (7.5, 95)	40 (8.5, 87.75)	22 (7.5, 100)	0.016
ESR (mm 1st hour), mean (SD)	69 (36)	74.3 (35.7)	60.7 (34.6)	0.030
CRP (mg/dl), mean (SD)	6.4 (5.9)	6.1 (5.3)	6.6 (6.6)	0.650
Symptoms duration at first imaging (weeks), median (Q1, Q3)	13 (5, 25.5)	17 (8, 31)	10 (4, 22.75)	0.090
LV Imaging modality				<0.0001
MRA	43 (27.4)	14 (32.6)	29 (67.4)	
PET/CT	114 (72.6)	79 (71.2)	32 (28.8)	
Diameter at first imaging	n 153	n 91	n 59	
Mid-ascending aorta (cm), mean (SD)	3.68 (0.43)	3.73 (0.45)	3.62 (0.40)	0.124
Aortic arch (cm), mean (SD)	3.06 (0.38)	3.12 (0.37)	2.95 (0.38)	0.005
Mid-descending aorta (cm), mean (SD)	2.91 (0.35)	2.97 (0.36)	2.81 (0.32)	0.008
Suprarenal aorta (cm), mean (SD)	2.32 (0.31)	2.39 (0.31)	2.23 (0.28)	0.001
Patients with prevalent aneurysms	30/153 (19.6)	23/91 (25.3)	7/59 (11.9)	0.05
Number of aortic segments with prevalent aneurysm				

1	27	21	6	
2	1	1	0	
3	2	1	1	
Median time between first and last imaging (months), median (Q1, Q3)	30 (17, 69.5)	38 (17, 76)	28 (14.5, 50.5)	0.093
Patients with relapses	60/151 (39.7)	31/87 (35.6)	28/61 (45.9)	0.209
Annual growth rate (mm^2/year) (mean, sd)	n 153	n 91	n 59	
Mid-ascending aorta (mm^2/year), mean (SD)	0.02 (0.11)	0.03 (0.11)	0.01 (0.11)	0.305
Aortic arch (mm^2/year), mean (SD)	0.03 (0.09)	0.02 (0.10)	0.03 (0.09)	0.554
Mid-descending aorta (mm^2/year), mean (SD)	0.02 (0.12)	0.02 (0.10)	0.01 (0.15)	0.609
Suprarenal aorta (mm^2/year), mean (SD)	0.00 (0.07)	0.00 (0.07)	0.01 (0.06)	0.271
Incident aneurysms				
Number of incident aneurysm	19	14	5	
Patients without aneurysm at baseline	*12*	*8*	*4*	
Patients with aneurysm at baseline	*7*	*6*	*1*	

*** Percentages are calculated only in patients who underwent TAB.**

Figure 5. Percentage of patients who underwent imaging within six months before or after diagnosis. Time is reported in weeks.

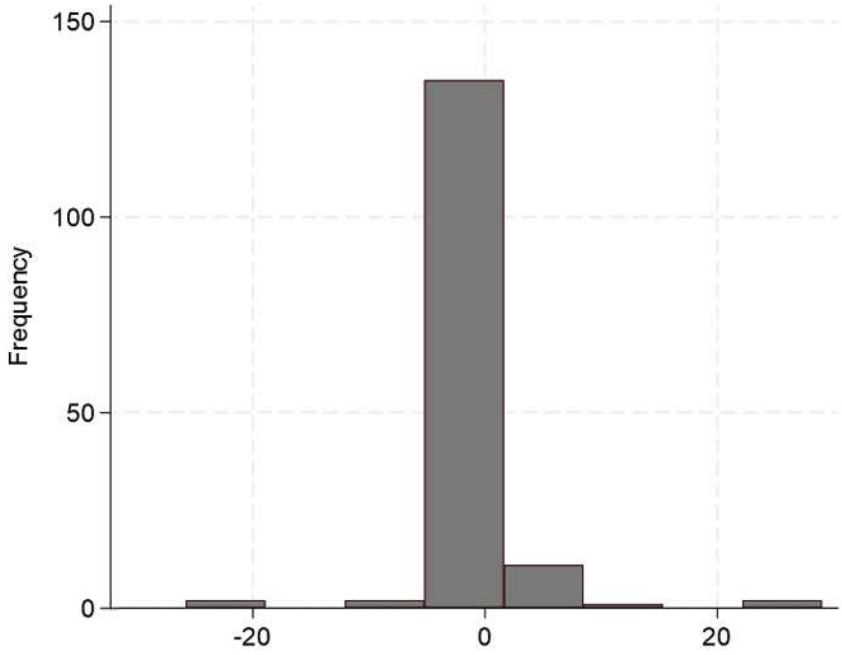

3.1.2. Baseline aortic diameter and aortic dilation

Patients with aortitis had significantly larger aortic diameters at baseline than those without aortitis in the aortic arch (3.12 vs. 2.95 cm; p=0.005), mid-descending aorta (2.97 vs. 2.81 cm; p=0.008), and suprarenal aorta (2.39 vs. 2.23 cm; p=0.001) (**Table1**).

In cross-sectional analyses, a larger baseline aortic diameter was independently associated with the presence of aortitis at both the patient level (β = 0.184; p<0.0001) and the aortic segment level (β = 0.154; p=0.001). In segment-level models, aortitis within a given district was significantly associated with larger diameter in the aortic arch (β = 0.130; p=0.030), mid-descending aorta (β = 0.158; p=0.003), and suprarenal aorta (β = 0.143; p=0.002).

In multivariable models, female sex (β = -0.304; p<0.0001), hypercholesterolemia (β = -0.134; p=0.003), visual symptoms (β = -0.190; p=0.003), and ischemic symptoms (β = -0.196; p<0.0001) were associated with smaller baseline aortic diameters (**Table2**).

Aortic aneurysms were identified in 30 patients (prevalence: 19.6%) and in 36 of 616 aortic segments (5.8%), most frequently involving the mid-ascending aorta (n=28). Aortitis was significantly associated with higher odds of prevalent aortic dilation, with a stronger effect at the patient level than the segment level (OR = 2.26; 95% CI: 1.00-5.11 vs. OR = 1.50; 95% CI: 0.69-3.25). Female sex and hypercholesterolemia were both associated with lower odds of prevalent aortic dilation (OR = 0.19; 95% CI: 0.09-0.40 and OR = 0.32; 95% CI: 0.13-0.80, respectively) (**Table2**).

Ten patients had baseline mid-ascending aorta aneurysm according to the ACC/AHA definition. The association between aortitis and prevalent aortic dilation remained significant when applying a threshold of 4.5 cm for the mid-ascending aorta (OR = 3.23 [95% CI: 0.85, 12.30]).

The results remained largely consistent when analyses were stratified by GC treatment status at baseline imaging. However, the association between aortitis and prevalent aortic dilation appeared

stronger among patients already receiving GCs (OR = 4.08; 95% CI: 1.06–9.94) than among untreated patients (OR = 2.03; 95% CI: 0.75–5.46).

Similarly, adjusting for study center (Reggio Emilia or Würzburg) and imaging modality (PET/CT or MRI) did not materially alter the findings (**Table 3**).

Table 2. Cross-sectional analyses (age and sex adjusted)

		Outcome: Diameter at baseline					Outcome: Prevalent aneurysm				
		n	Coeff	p	95%CI		events	OR	p	95%CI	
Patient level	**Age at Imaging**	616	0.003	0.278	-0.002	0.008	36	1.01	0.72	0.96	1.06
	Female	428	-0.304	0.000	-0.411	-0.197	12	0.19	0.00	0.09	0.40
	Hypercholesterolemia	224	-0.134	0.003	-0.223	-0.045	6	0.32	0.02	0.13	0.80
	Hypertension	388	-0.008	0.863	-0.097	0.081	22	0.78	0.49	0.38	1.58
	Diabetes	76	-0.036	0.615	-0.175	0.104	4	0.81	0.71	0.27	2.40
	Current smoker	144	-0.009	0.874	-0.116	0.098	7	0.66	0.43	0.23	1.87
	Visual symptoms	92	-0.190	0.003	-0.316	-0.065	3	0.39	0.12	0.11	1.30
	Ischemic symptoms	172	-0.196	0.000	-0.291	-0.102	6	0.46	0.10	0.19	1.16
	Systemic symptoms	364	-0.001	0.980	-0.089	0.087	25	1.18	0.66	0.56	2.49
	Cranial symptoms	316	-0.085	0.070	-0.177	0.007	15	0.63	0.23	0.29	1.34
	PMR	172	-0.031	0.551	-0.134	0.072	7	0.69	0.40	0.30	1.63
	Aortitis	368	0.184	0.000	0.099	0.268	26	2.26	0.05	1.00	5.11
Aortic segment level	**Aortitis by district overall**	310	0.154	0.001	0.063	0.245	20	1.50	0.30	0.69	3.25
	Aortitis by district										
	Mid-ascending aorta	77	0.100	0.133	-0.031	0.230					
	Aortic arch	80	0.130	0.030	0.012	0.248					
	Mid-descending aorta	81	0.158	0.003	0.054	0.262					
	Suprarenal aorta	72	0.143	0.002	0.055	0.231					

Table 3. Cross-sectional analyses adjusted by age, sex, center and imaging modality

		Outcome: Diameter at baseline					Outcome: Prevalent aortic dilation				
		n	Coeff	p	95%CI		events	OR	p	95%CI	
Patient level	**Aortitis**	368	0.167	0.000	0.082	0.252	26	2.25	0.07	0.94	5.38
Aortic segment level	**Aortitis by district overall**	310	0.150	0.002	0.058	0.242	20	1.53	0.32	0.66	3.54
	Aortitis by district										
	Mid-ascending aorta	77	0.107	0.128	-0.031	0.244					
	Aortic arch	80	0.130	0.030	0.012	0.248					
	Mid-descending aorta	81	0.154	0.003	0.054	0.255					
	Suprarenal aorta	72	0.166	0.000	0.077	0.254					

3.1.3.Longitudinal outcomes

The median time between the first and last imaging was 30 months. The distribution of patients by time from first to last imaging is shown in Supplementary **Figure 6**. There was a significant increase in aortic diameters between the first and last imaging (mean change 0.11 cm at the mid-ascending aorta, P < 0.0001; 0.09 cm at the aortic arch, P< 0.0001; 0.09 cm at the descending aorta, P< 0.0001; 0.02 cm at the suprarenal aorta, P = 0.099) without difference between patients with and without aortitis. Mean annual expansion rates of the aortic area ranged from 0.00 to 0.03 cm2 /year, again without differences between patients with and without baseline aortitis (**Table 1**). At follow-up imaging, new aortic dilation was identified in 12 of 123 patients without baseline dilation (incidence: 9.8%) and in 24 of 580 not dilated aortic segments (4.1%), most frequently involving the mid-ascending aorta (n = 13) (**Table 4**). Baseline aortic diameter was the strongest predictor of aortic area increase (β = 0.088, P = 0.006) and incident aortic dilation development (HR 3.85 [95% CI: 2.02, 7.32]). In multivariable models, visual symptoms were associated with smaller aortic area increase (β = −0.111; P = 0.038), while neither baseline aortitis nor other clinical variables were independently associated with aortic expansion or incident aortic dilation development (**Table 5**). At follow-up imaging, 8 patients developed a new mid-ascending aorta aneurysm according to ACC/AHA definition. Baseline aortic diameter remained the only predictor of incident aortic dilation when applying a threshold of 4.5 cm for the mid-ascending aorta (HR 3.83 [95% CI: 1.76, 8.35]).

Interestingly, when analyses were stratified by GC treatment status at the time of baseline imaging, aortitis had a stronger, although not significant, effect on the risk of developing a new aortic dilation during follow-up in patients who were treated (HR 3.19 [95% CI: 0.65, 15.67]) compared with those who were not (HR 0.48 [95% CI: 0.09, 2.38]). The effect was confirmed at the overall segment level in the velocity of aortic area increase (β = 0.098, P = 0.074), with a larger effect in the aortic arch (β

= 0.212, P = 0.026) (**Table 5**). Adjusting for study centre (Reggio Emilia or Würzburg) and imaging modality (PET/CT or MRI/MRA) did not alter the findings (**Table 6**).

Figure 6. Distribution of patients according to the time from first to last imaging

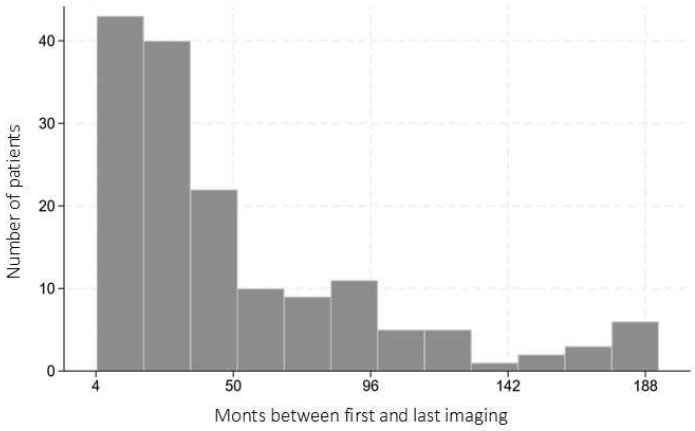

Table 4. Aneurysms by aortic segment

	Prevalent	In regression	Incident	Never
Overall	36	2	24	556
Aortic segment				
Mid-ascending aorta	28	2	13	113
Aortic arch	2	0	4	148
Mid-descending aorta	1	0	4	149
Suprarenal aorta	5	0	3	146

Table 5. Longitudinal Analyses on incident outcomes (age and sex adjusted)

		Outcome: New aneuriysm						Outcome: Velocity in area increase				
		n	events	HR	p	95%CI		n	Coeff	p	95%CI	
Patient level	**Age at Imaging**	628	24	1.07	0.01	1.01	1.12	611	0.000	0.866	-0.005	0.004
	Female	436	14	0.54	0.20	0.21	1.38	427	0.006	0.882	-0.077	0.090
	Hypercholesterolemia	224	5	0.59	0.33	0.20	1.70	224	-0.077	0.061	-0.157	0.004
	Hypertension	396	14	0.94	0.92	0.30	2.94	387	-0.083	0.064	-0.170	0.005
	Diabetes	76	5	1.87	0.43	0.40	8.68	75	0.006	0.955	-0.208	0.220
	Current smoker	148	3	0.58	0.48	0.13	2.57	413	0.031	0.499	-0.060	0.122
	Visual symptoms	96	1	0.61	0.65	0.07	5.16	92	-0.111	0.038	-0.216	-0.006
	Ischemic symptoms	176	4	1.16	0.85	0.26	5.16	172	-0.059	0.214	-0.152	0.034
	Systemic symptoms	364	13	1.58	0.36	0.60	4.16	364	0.073	0.079	-0.009	0.155
	Cranial symptoms	324	13	1.50	0.42	0.57	3.93	316	0.009	0.827	-0.075	0.093
	PMR	172	4	0.52	0.29	0.15	1.76	172	-0.057	0.145	-0.135	0.020
	Aortitis	372	15	1.07	0.90	0.35	3.27	367	0.011	0.821	-0.086	0.108
Aortic segment level	**Aortitis by district overall**	314	12	0.88	0.81	0.31	2.47	305	0.019	0.674	-0.071	0.109
	Diameter (cm)	616	24	3.85	0.00	2.02	7.32	611	0.088	0.006	0.026	0.151
	Aortitis by district (adjusted by age, sex and baseline diameter)											
	Mid-ascending aorta							76	0.116	0.233	-0.076	0.308
	Aortic arch							78	0.083	0.159	-0.033	0.199
	Mid-descending aorta							80	-0.072	0.341	-0.221	0.077
	Suprarenal aorta							71	-0.039	0.260	-0.108	0.029

Table 6. Longitudinal Analyses on incident outcomes adjusted by age, sex, center and imaging modality

		Outcome: New aortic dilation						Outcome: Velocity in area increase				
		n	**events**	**HR**	**p**	**95%CI**		**n**	**Coeff**	**p**	**95%CI**	
Patient level	**Aortitis**	372	15	1.38	0.55	0.48	3.94	367	-0.018	0.682	-0.106	0.069
Aortic segment level variables	**Aortitis by district overall**	314	12	1.09	0.86	0.40	3.01	305	0.017	0.698	-0.068	0.101
	Diameter (cm)	616	24	3.91	0.00	2.12	7.22	611	0.077	0.017	0.014	0.140
	Aortitis by district (adjusted by age, sex and baseline diameter)											
	Mid-ascending aorta							76	0.113	0.196	-0.059	0.286
	Aortic arch							78	0.111	0.088	-0.017	0.239
	Mid-descending aorta							80	-0.135	0.063	-0.277	0.007
	Suprarenal aorta							71	-0.047	0.193	-0.118	0.024

3.2. The role of TIVV and TIGV as diagnostic and prognostic biomarkers

3.2.1. Cohort description

Baseline features of the cohort are reported in **Table 7**. Eighteen patients were included from March 2019 to November 2020, and 10 completed follow-up through week 78. Eight patients dropped out before week 78: two before week 24 due to nonresponse to treatment; one at week 29 due to withdrawal of informed consent; one at week 44 due to adverse events (aortic aneurysm surgical repair); and four due to disease relapse at weeks 24 (PMR, persistent grade 3 FDG uptake), 52 (low-grade fever, elevation of CRP, persistent grade 2 FDG uptake), 60 (systemic symptoms, elevation of CRP), and 74 (PMR, elevation of CRP). Three patients showed aortic dilatation (two at week 24 and one at week 52). Following EULAR consensus definitions, the proportion of patients in remission at weeks 24, 52, and 78 was 13/18 (72%), 10/17 (59%), and 8/17 (47%), respectively. Three additional patients relapsed after the 6-month observational period, at 38 weeks (PMR, elevation of CRP), 76 weeks (fever, elevation of CRP), and 96 weeks (PMR, elevation of CRP) after tocilizumab discontinuation. At the most recent visit in our Vasculitic Clinic, after a median (Q1, Q3) follow-up of 148 (64, 178) weeks from tocilizumab discontinuation, 5/17 patients (29%) remained in relapse-free remission.

A total of 61 PET scans were included in this study.

The mean TIVV values were 82 (SD 67) and 262 (SD. 181) for remission and active disease, respectively. For TIGV, the mean values were 187 (SD 153) and 608 (SD 414) for remission and active disease, respectively.

The mean PETVAS scores were 9.0 (SD 4.5) and 15.2 (SD 5.6) for remission and active disease, respectively. The mean TVS scores were 6.7 (SD 3.4) and 10.8 (SD 4.4) for remission and active disease, respectively.

The mean SUVmean values were 2.29 (SD 0.31) and 2.40 (SD 0.36) in remission and active disease, respectively. The mean SUVmean G3 values were 2.76 (SD 0.38) and 2.78 (SD 0.35) in remission and active disease, respectively. The mean SUVmax values were 4.32 (SD 1.87) and 5.28 (SD 1.58) in remission and active disease, respectively.

At baseline, 4 patients had a visual score of grade 2 and 14 had a visual score of grade 3. At week 24, 3 patients had a visual score of grade 2 and 4 had a visual score of grade 3. At week 56, 3 patients had a visual score of grade 2 and 1 had a visual score of grade 3.

At week 76, 3 patients had a visual score of grade 2 and 2 had a visual score of grade 3.

Table 7. Baseline characteristics of the enrolled patients

Study population (n=18)	
Age, years	68.5 (10.6)
Sex	
Female	13 (72%)
Male	5 (28%)
Ethnic origin	
White	18 (100%)
Newly diagnosed LV-GCA	9 (50%)
Relapsing LV-GCA	9 (50%)
Glucocorticoid pre-treatment	13 (72%)
CRP, mg/L	35 (36)
ESR, mm/h	56 (41)
Symptoms of active vasculitis	15 (83%)
PETVAS	17.3 (5.1)
TVS	12.3 (4.5)
Visual score	
Visual score 2	4 (22%)
Visual score 3	14 (78%)
TIVV, ml	309 (180.9)
$TIVV_{G3}$, ml	112 (92.2)
SUV_{mean}	2.41 (0.43)
$SUV_{mean\ G3}$	2.72 (0.38)
SUV_{max}	5.48 (1.70)
TIGV, ml	725 (424.8)
$TIGV_{G3}$, ml	314 (280.1)

Data are mean (SD) or n (%)

3.2.2. Diagnostic role of PET metrics

Of the 61 PET/CT scans, 29 were performed in patients with active disease (18/18 at baseline, 4/17 at week 24, 4/15 at week 52, and 3/11 at week 78) (**Figure 7**).

In the cross-sectional regression analysis excluding baseline PET/CT scans, TIVV and TIGV were strongly associated with active disease, with ORs of 4.74 (95% CI 1.23–18.2) and 5.45 (95% CI 1.36–21.8), respectively. Additionally, the visual score, PETVAS, and TVS showed moderate associations with the outcome, with ORs of 2.26 (95% CI 0.94–5.44), 2.16 (95% CI 0.87–5.33), and 1.86 (95% CI 0.76–4.52), respectively. However, these OR estimates were imprecise, and the differences might be due to chance. Conversely, SUVmax, SUVmean, and SUVmean G3 showed weaker associations with the outcome, with ORs largely compatible with random fluctuations: 1.41 (95% CI 0.73–2.75), 1.52 (95% CI 0.69–3.34), and 1.37 (95% CI 0.68–2.75), respectively (**Table 8**). Similar results were observed when all 61 PET/CT scans were included: ORs for TIVV and TIGV were 10.94, 95%CI 3.07-38.97; 11.61, 95%CI 3.19-42.33, respectively. ORs for PETVAS and TVS were 4.35, 95%CI 1.94-9.80 and 3.49, 95%CI 1.64-7.45, respectively. The differences in PET parameters between active and non-active disease did not change when analyses were conducted at the different time points (week 24, week 52 and week 76).

Figure 7. PET/CT view of a patient followed longitudinally at various time points: (A) anterior view in a patient with active disease and high TIVV; (B, C) MIP anterior view showing disease remission; (D) anterior view demonstrating relapse; (E) PETVAS and TVS scores. (F) TIVV value.

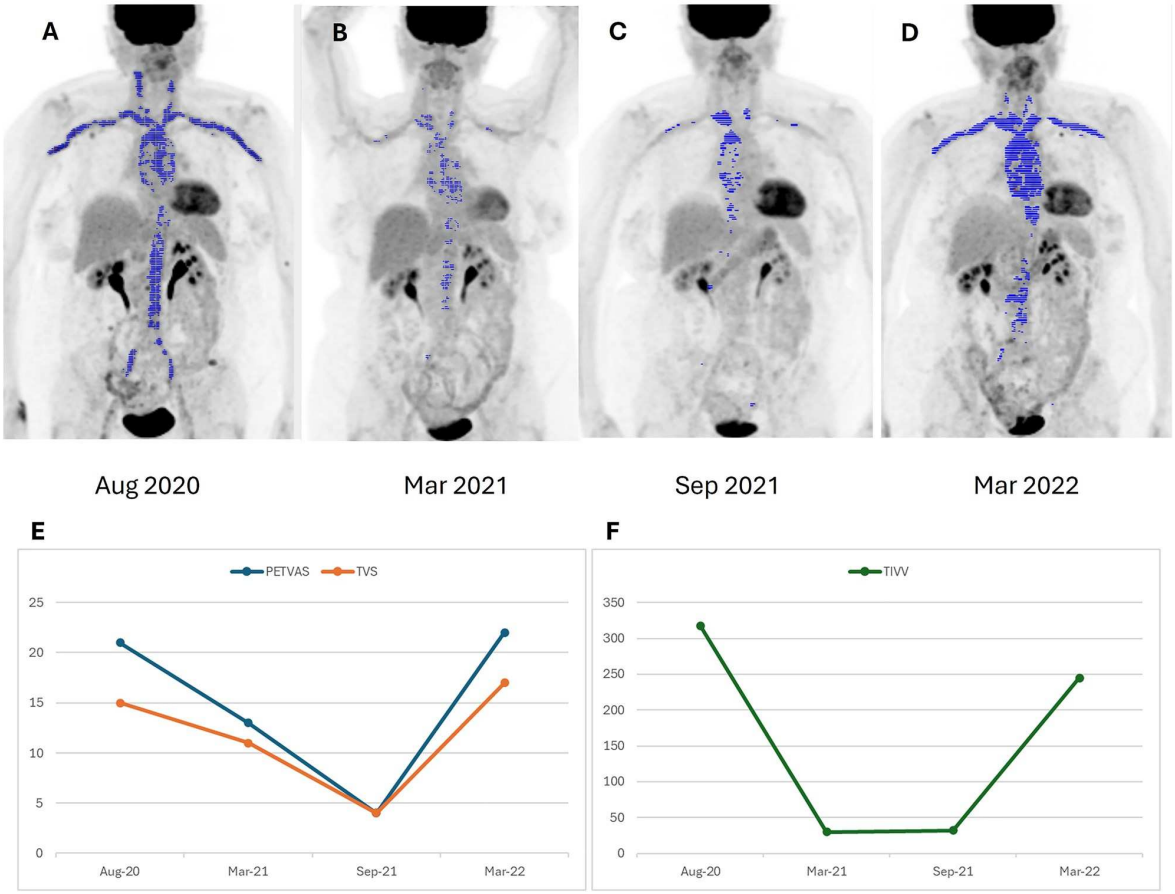

Table 8. ORs of having active disease for different PET parameters. Cross-sectional analysis. ORs are expressed for the increase of a standard deviation of standardized variables, unless otherwise specified.

		Active disease								
		NO			YES			Cross-sectional analysis		
		N %	Mean	SD	N %	Mean	SD	Odds Ratio	95%CI	P-value
Total		**32 74.4**			**11 25.6**					
Age			67.8	8.4		68.0	13.0			
PETVAS			9.0	4.5		11.8	4.7	2.16	0.87-5.33	0.095
TVS			6.7	3.4		8.3	3.0	1.86	0.76-4.52	0.173
***Visual Score**										
	1	23 71.9			4 36.4			2.26	0.94-5.44	0.068
	2	5 15.6			4 36.4					
	3	4 12.5			3 27.2					
TIVV			82.2	66.5		183.7	158.0	4.74	1.23-18.2	0.023
$TIVV_{G3}$			15.9	22.9		47.7	53.9	5.18	1.22-22.0	0.026
SUV_{mean}			2.3	0.3		2.4	0.2	1.52	0.69-3.34	0.299
$SUV_{mean\ G3}$			2.8	0.4		2.9	0.3	1.37	0.68-2.75	0.381
SUV_{max}			4.3	1.9		5.0	1.4	1.41	0.73-2.75	0.305
TIGV			187.3	152.6		418.3	331.6	5.45	1.36-21.8	0.017
$TIGV_{G3}$			42.2	61.6		129.7	145.8	6.11	1.26-29.6	0.025

*Non-standardized variable. Odds ratio is reported for unit increase.

3.2.3. Prognostic role of PET metrics

Over a median (Q1, Q3) follow-up of 117 (56, 204.5) weeks, 7 patients experienced disease relapse and 3 developed aortic dilatations, for a total of 10 events. The Cox hazard model showed strong associations of TIVV and TIGV with time to relapse or aortic dilatation, with HRs of 2.50 (95% CI 1.07–5.84) and 2.23 (95% CI 1.04–4.82), respectively.

In contrast, PETVAS and TVS showed weaker associations with prognosis (HR 1.79; 95% CI 0.84–3.80 and HR 1.27; 95% CI 0.67–2.39, respectively), while visual score, SUVmean, and SUVmax showed weak, if any, associations with the outcome, with HRs near 1 (**Table 9**). When aortic dilatation was excluded from the outcome definition, the association between TIVV and TIGV and time to relapse was weak (HR 1.34, 95%CI 0.46-288; HR 1.06, 95%CI 0.40-2.86, respectively). On the other hand, all three patients who developed aortic dilatation showed markedly elevated inflammatory PET metrics at baseline, particularly TIVV and TIGV with a mean of 517.7 (SD 1.7) and 1319 (SD 584.9), respectively. These findings suggest a potential strong association between the initial inflammatory burden detected by PET/CT and the subsequent development of aortic dilatation.

Finally, an analysis was performed to evaluate the prognostic significance of early changes in PET parameters (delta), i.e., differences between baseline (t0) and week 24 (t24). The Cox models lacked sufficient statistical power to achieve acceptable precision for HRs; nevertheless, the only HRs with high values were for visual score (HR 3.86, 95%CI 0.41-36.27), TIVV (HR 1.90, 95%CI 0.06-57.38), and TIGV (HR 1.81, 95%CI 0.08-41.66). When aortic dilatation was excluded from the outcome definition, associations between changes in visual score (HR 13.99, 95%CI 0.69-283.83), TIVV (HR 8.80, 95%CI 0.08-943.89), and TIGV (particularly TIVVG3 [HR 316.08, 95%CI 0.49-205315.00] and TIGVG3 [HR 22.81, 95%CI 0.57-918.43]) and subsequent relapse became stronger, albeit imprecise. These findings suggest a potential role for early reduction of TIVVG3 in lowering the risk of relapse. **Figure 8** represents the correlation matrix of PET parameters.

Table 9. Hazard ratios of having relapse or aortic dilatation during follow up for different PET parameters measured at baseline. HRs are expressed for the increase of a standard deviation of standardized variables, unless otherwise specified.

		Relapse or aortic dilatation								
		NO			YES			Longitudinal analysis		
		N %	Mean	SD	N %	Mean	SD	Hazard Ratio	95%CI	P-value
Total		**6** **37.5**			**10** **62.5**					
Age			64.8	10.6		71.4	8.9	1.07	0.98-1.17	0.119
PETVAS			15.2	4.1		20.1	4.1	1.79	0.84-3.80	0.133
TVS			11.0	4.1		14.1	4.2	1.27	0.67-2.39	0.463
***Visual Score**										
	1	0 0			0 0			1.50	0.18-12.2	0.704
	2	2 33.3			1 10					
	3	4 66.7			9 90					
TIVV			257.5	104.1		380.9	197.6	2.50	1.07-5.84	0.035
$TIVV_{G3}$			90.8	66.7		142.4	102.3	1.91	0.89-4.11	0.097
SUV_{mean}			2.3	0.5		2.5	0.4	1.42	0.71-2.83	0.313
$SUV_{mean\ G3}$			2.6	0.5		2.8	0.4	1.19	0.62-2.28	0.594
SUV_{max}			5.2	1.6		5.4	1.2	1.06	0.41-2.77	0.898
TIGV			582.7	233.1		903.8	460.4	2.23	1.04-4.82	0.039
$TIGV_{G3}$			250.5	218.1		400.5	311.2	1.76	0.84-3.63	0.129

*Non-standardized variable. Hazard ratio is reported for unit increase.

Figure 8. Correlation matrix among PET parameters

	PETVAS	Visual Score	$TIVV_{G3}$	TIVV	$SUV_{mean\ G3}$	SUV_{mean}	SUV_{max}	$TIGV_{G3}$	TIGV	TVS
PETVAS	1									
Visual Score	0,793	1								
$TIVV_{G3}$	0,786	0,647	1							
TIVV	0,716	0,627	0,852	1						
$SUV_{mean\ G3}$	0,063	0,076	0,013	-0,147	1					
SUV_{mean}	0,223	0,196	0,174	0,015	0,753	1				
SUV_{max}	0,411	0,463	0,457	0,409	0,389	0,239	1			
$TIGV_{G3}$	0,776	0,628	0,993	0,809	0,088	0,24	0,474	1		
TIGV	0,766	0,652	0,909	0,978	-0,01	0,153	0,467	0,888	1	
TVS	0,937	0,795	0,781	0,672	0,155	0,298	0,423	0,782	0,735	1

4. DISCUSSION

This work enhances our understanding of the relationship between inflammation and subsequent vascular damage in GCA by examining the role of imaging in clinical management, especially in patients with LV-GCA. Our findings emphasize that imaging should be viewed not just as a diagnostic tool but as a vital part of disease characterization, prognostic assessment, and ongoing monitoring. Importantly, the study integrates two complementary aspects of imaging: assessing structural vascular damage and quantifying inflammatory burden.

In the cohorts from Reggio Emilia and Würzburg, aortic involvement was common at diagnosis, with 60% of patients showing aortitis, often affecting the entire aorta (panaortitis), and 20% already displaying early aortic dilation, most frequently in the mid-ascending aorta. After a median follow-up of 30 months, 10% of patients without initial dilation developed new dilation, mainly involving the mid-ascending aorta. Patients with GCA have a 3- to 17-fold increased risk of developing thoracic aortic aneurysms. Aortic dilatation may occur early or late in the disease, affecting 15–23% of newly diagnosed patients and 22.2% to 33.3% of patients after a median disease duration of 5.4 and 10.3 years, respectively (88–90,96,99–102). The prevalence and incidence of aortic dilation in our study are consistent with these findings.

Baseline aortitis was linked to larger aortic diameters and the presence of aneurysms at diagnosis. However, it did not independently predict the development of aneurysms or continued aortic growth during follow-up. Instead, baseline aortic diameter was the strongest predictor for future aneurysm formation and ongoing aortic enlargement.

Our results align partially with four retrospective studies indicating that FDG uptake in large vessels at diagnosis correlates with an increased risk of future aortic complications (102–105). Supporting this, a recent prospective study of 106 patients evaluated vascular FDG uptake at diagnosis and its relationship with changes in aortic size. After a median of 6 years, patients with positive baseline

PET scans showed greater increases in thoracic aortic diameter and a higher incidence of thoracic aortic aneurysms compared to those with negative scans (106). These findings suggest that vascular FDG uptake at diagnosis is an independent risk factor for the development of thoracic aortic aneurysms in GCA. The fact that baseline aortic diameter was the strongest predictor in the Reggio Emilia and Würzburg cohorts for both incident aortic dilation and progressive aortic expansion, however, supports the importance of baseline aortic measurements for risk stratification.

Notably, our finding that greater baseline inflammatory volume (TIVV and TIGV) is associated with aortic dilation suggests that overall inflammatory burden may have a greater impact than regional FDG uptake in predicting aortic dilatation. This underscores the potential of TIVV and TIGV as valuable prognostic tools in clinical practice, offering a more sensitive approach to monitoring disease progression and therapeutic response.

Furthermore, the utility of FDG PET/CT in predicting future relapses in LVV patients remains debated (94). The latest EULAR guidelines do not currently recommend PET/CT for monitoring treatment, although they recognize the need for an objective tool to assess disease activity during follow-up (48). Many studies have not found a link between baseline PET parameters (whether visual, semi-quantitative, or quantitative) and subsequent relapses, some report an association between PETVAS during clinical remission and future flare-ups (73). Consistent with these findings, baseline PET parameters (TVS, PETVAS, SUV, TIVV and TIGV) showed only weak correlations with relapse risk. However, early changes in high-grade inflammatory volume (specifically delta TIVVG3 and delta TIGVG3) appeared to be associated with future disease recurrence. Although these findings are preliminary due to limited sample size, they suggest that dynamic shifts in inflammatory burden during treatment may hold more prognostic value than static baseline measurements. This indicates a potential role for PET imaging not only in monitoring therapy but also in early identification of patients at higher risk of relapse. These findings parallel recent advancements in oncology PET

imaging, in which metabolic tumour volume has demonstrated superior prognostic accuracy compared with traditional metrics, highlighting the growing utility of volumetric and metabolic measures in chronic disease management (107,108).

A key methodological factor between the two cohorts involves GC therapy prior to imaging. It is well known that GCs rapidly reduce vascular FDG uptake, particularly within the first 3–10 days of high-dose treatment (75). In the retrospective cohorts of Reggio Emilia and Würzburg, 40% of patients had already started GC therapy before baseline imaging, although the doses were relatively low and more typical of PMR than vasculitis (average prednisone dose: 17 mg/day; median treatment duration: 30 days). This may partly explain differences between our findings and earlier studies. Conversely, TIVV and TIVG were assessed in PET/CT scans performed according to protocol in the TOPAZIO study, where all patients received three boluses of methylprednisolone and tocilizumab monotherapy (87). Although the re-evaluation was retrospective, the cohort was homogeneous regarding imaging protocols, treatments, and follow-up.

Variations in follow-up duration, GC exposure, and timing of imaging are likely to significantly influence the prognostic effectiveness of inflammatory imaging.

Interestingly, in the retrospective cohorts from Reggio Emilia and Würzburg persistent aortitis despite GC treatment was linked to existing aneurysms and showed a trend toward association with new aneurysm development in treated patients. This suggests that PET-positive aortitis post-treatment may identify a subgroup with steroid-resistant or inadequately managed vascular inflammation, possibly at higher risk for structural complications. Subclinical LVV has been reported in up to 23% of PMR patients, raising concerns about hidden vascular inflammation and long-term damage (109–112). Case reports and small series have documented PMR patients developing aortic aneurysms over time, supported by recent histopathological evidence. In a retrospective study of 4.621 patients undergoing thoracic aortic repair, 43 had a history of isolated PMR, with active aortic

inflammation found in 70% of them, even up to ten years after diagnosis (113). These findings suggest that subclinical LVV is likely under-recognized in PMR and may contribute to aortic complications.

Furthermore, patients with aortitis in the Reggio Emilia and Würzburg cohorts tended to be younger and less frequently exhibited cranial or ischemic symptoms, often experiencing longer delays in diagnosis. These findings align with previous research, including the study by Moreel et al. (103,106,114,115). Such a phenotype reflects earlier descriptions of a systemic or PMR-like presentation in patients with predominant large-vessel involvement (7). Hence, the link between aortitis and increased baseline aortic diameter may indicate diagnostic delays in this subgroup, who often show systemic features or refractory PMR but lack classical cranial signs. This supports the idea that prolonged vascular inflammation can cause early structural damage by the time of diagnosis. Although current evidence does not support routine vascular imaging or long-term aortic monitoring for all PMR patients, targeted imaging may be beneficial for selected cases, especially those with relapsing, refractory, or atypical disease.

In patients with active LV-GCA, TIVV and TIGV also showed a stronger relationship with clinical disease activity than traditional qualitative or semi-quantitative parameters such as PETVAS, TVS, or SUV-based metrics. One prior study evaluated the diagnostic accuracy of TIVV and TIGV for detecting active disease in a retrospective cohort of 36 patients with Takayasu arteritis (116). Both TIVV and TIGV exhibited excellent intra- and inter-rater reliability. Receiver Operating Characteristic (ROC) curves, based on absolute values, produced similar area under the curve (AUC) results to physician global assessments, across metrics such as SUVmax, SUVmean, TBR, TIVV, TIGV, and PETVAS.

The main methodological difference between the two studies lies in how TIVV was calculated. Ora et al. drew ROIs where FDG uptake exceeded a SUVmean threshold of 1.5. In our study, we used the

liver SUVmean as the cutoff. This allowed us to classify inflammation volume based on severity and to compute both TIVV and TIVVG3, which represent volumes with inflammation at or above, and strictly above, the liver's SUVmean, respectively.

This approach, grounded in the validated visual grading score, appears to offer strong diagnostic and prognostic accuracy. Parameters for TIVV and TIGV that include both grade 2 and 3 volumes were similarly associated with disease activity, compared to those considering only grade 3 volumes. Moreover, baseline TIVV and TIGV that encompass both grades demonstrated superior performance in predicting future relapse and vascular damage compared to metrics limited to grade 3 volumes.

Consistent with prior research, SUVmax and SUVmean alone did not show a significant association with disease activity. This highlights an important pathophysiological point: GCA is a systemic inflammatory condition characterized by widespread vascular involvement rather than localized hypermetabolic lesions. Therefore, relying solely on peak uptake measures may not accurately represent the overall inflammatory burden. In contrast, volumetric-metabolic parameters encompass both the extent and intensity of vascular inflammation, offering a more comprehensive view of disease activity.

Strengths of the study include its multicenter design, standardized data collection, and comprehensive imaging assessment incorporating both PET/CT and MRI/MRA. The segment-level analysis used in the first part of the study further enhances the resolution of anatomical patterns, providing detailed insights into aortic involvement in GCA.

Nevertheless, several limitations must be acknowledged. First, the retrospective design of the first part of the project and the unblinded retrospective re-analysis of the PET/CT scans performed in the TOPAZIO by a single nuclear medicine physician.

Additionally, although two different cohorts were used in the first part, imaging was interpreted locally at each site, which may have introduced variability in measurement techniques and reduced inter-site consistency.

The duration of follow-up, while adequate to detect early changes, may have been insufficient to fully capture long-term complications such as aneurysm formation. Moreover, the use of low-dose GCs in the retrospective cohorts prior to baseline imaging raises concerns about potential under-treatment of vascular inflammation, which could have influenced both imaging findings and outcomes.

In the second part of the project, the use of GCs was standardized, but the sample size was small.

An additional limitation concerns the semiautomatic approach employed. Although TIVV and TIGV serve as quantitative parameters, their computation still requires manual input, which introduces potential variability and increases the time burden. However, their quantitative nature makes them strong candidates for full automation. Recently, robust and precise artificial intelligence models for organ segmentation have emerged, capable of delineating large vessels on CT scans, including those with low-dose, non-contrast enhancement (117). By using these segmentations, quantitative metrics can be computed from PET overlays, enabling swift analysis across large datasets. Nonetheless, establishing standardized metrics for consistent evaluation remains crucial, along with generating substantial evidence to support the efficacy of these quantitative approaches.

5. CONCLUSIONS

In conclusion, this study advocates for a comprehensive imaging-based approach to GCA that combines quantification of inflammatory burden with assessment of vascular structure. The baseline aortic diameter stands out as the most reliable predictor of future aneurysm development, highlighting the importance of structural evaluation at diagnosis. Volumetric PET parameters such as TIVV and TIGV seem to offer a more accurate reflection of disease activity than traditional qualitative metrics and may provide early prognostic insights into relapse and vascular dilation. These results indicate that inflammation triggers vascular injury, while long-term disease progression is shaped by structural remodeling and mechanical factors. By integrating metabolic and morphological imaging, we can enhance personalized risk assessment and improve strategies for ongoing surveillance in patients with LV-GCA.

REFERENCES

1. Jennette JC, Falk RJ, Bacon PA, Basu N, Cid MC, Ferrario F, et al. 2012 Revised International Chapel Hill Consensus Conference Nomenclature of Vasculitides. Arthritis Rheum. 2013 Jan;65(1):1–11. doi:10.1002/art.37715

2. Ponte C, Grayson PC, Robson JC, Suppiah R, Bates Gribbons K, Judge A, et al. 2022 American College of Rheumatology/EULAR classification criteria for giant cell arteritis. Ann Rheum Dis. 2022;81:1647–53. doi:10.1136/ard-2022-223480

3. HORTON BT, MAGATH TB, BROWN GE. ARTERITIS OF THE TEMPORAL VESSELS: A PREVIOUSLY UNDESCRIBED FORM. Arch Intern Med. 1934 Mar 1;53(3):400–9. doi:10.1001/archinte.1934.00160090077007

4. Kogstad OA. Polymyalgia rheumatica and its relation to arteritis temporalis. Acta Med Scand. 1965 Nov;178(5):591–8. PubMed PMID: 5850337.

5. Gilmour JR. Giant-cell chronic arteritis. J Pathol Bacteriol. 1941;53(2):263–77. doi:10.1002/path.1700530210

6. Hamrin B, Jonsson N, Hellsten S. “Polymyalgia arteritica”. Further clinical and histopathological studies with a report of six autopsy cases. Ann Rheum Dis. 1968;27(5):397–405. doi:10.1136/ard.27.5.397 PubMed PMID: 5677163.

7. Muratore F, Kermani TA, Crowson CS, Green AB, Salvarani C, Matteson EL, et al. Large-vessel giant cell arteritis: a cohort study. Rheumatology. 2015 Mar 1;54(3):463–70. doi:10.1093/rheumatology/keu329 PubMed PMID: 25193809.

8. Watts RA, Hatemi G, Burns JC, Mohammad AJ. Global epidemiology of vasculitis. Nat Rev Rheumatol 2021 181. 2021 Dec 1;18(1):22–34. doi:10.1038/s41584-021-00718-8 PubMed PMID: 34853411.

9. Salvarani C, Crowson CS, O’Fallon WM, Hunder GG, Gabriel SE. Reappraisal of the epidemiology of giant cell arteritis in Olmsted County, Minnesota, over a fifty-year period. Arthritis Rheum. 2004 Apr 15;51(2):264–8. doi:10.1002/art.20227 PubMed PMID: 15077270.

10. Muratore F, Boiardi L, Mancuso P, Restuccia G, Galli E, Marvisi C, et al. Incidence and prevalence of large vessel vasculitis (giant cell arteritis and Takayasu arteritis) in northern Italy: A population-based study. Semin Arthritis Rheum. 2021 Aug 1;51(4):786–92. doi:10.1016/J.SEMARTHRIT.2021.06.001 PubMed PMID: 34148007.

11. Carmona FD, Coit P, Saruhan-Direskeneli G, Hernández-Rodríguez J, Cid MC, Solans R, et al. Analysis of the common genetic component of large-vessel vasculitides through a meta-Immunochip strategy. Sci Rep 2017 71. 2017 Mar 9;7(1):1–11. doi:10.1038/srep43953 PubMed PMID: 28277489.

12. Weyand CM, Goronzy JJ. Immune mechanisms in medium and large-vessel vasculitis. Nat Rev Rheumatol. 2013 Nov 5;9(12):731–40. doi:10.1038/nrrheum.2013.161

13. Smeeth L, Cook C, Hall AJ. Incidence of diagnosed polymyalgia rheumatica and temporal arteritis in the United Kingdom, 1990-2001. Ann Rheum Dis. 2006 Aug;65(8):1093–8. doi:10.1136/ard.2005.046912 PubMed PMID: 16414971; PubMed Central PMCID: PMC1798240.

14. Ostrowski RA, Metgud S, Tehrani R, Jay WM. Varicella Zoster Virus in Giant Cell Arteritis: A Review of Current Medical Literature. Neuro-Ophthalmol. 2019 Jun;43(3):159–70. doi:10.1080/01658107.2019.1604763 PubMed PMID: 31312240; PubMed Central PMCID: PMC6620003.

15. Nordborg E, Nordborg C. Giant cell arteritis: epidemiological clues to its pathogenesis and an update on its treatment. Rheumatology. 2003 Mar;42(3):413–21. doi:10.1093/rheumatology/keg116 PubMed PMID: 12626790.

16. Mohan SV, Liao YJ, Kim JW, Goronzy JJ, Weyand CM. Giant cell arteritis: immune and vascular aging as disease risk factors. Arthritis Res Ther. 2011 Aug 2;13(4):231. doi:10.1186/ar3358 PubMed PMID: 21861860; PubMed Central PMCID: PMC3239337.

17. Watanabe R, Berry GJ, Liang DH, Goronzy JJ, Weyand CM. Pathogenesis of Giant Cell Arteritis and Takayasu Arteritis-Similarities and Differences. Curr Rheumatol Rep. 2020 Aug 26;22(10):68. doi:10.1007/s11926-020-00948-x PubMed PMID: 32845392; PubMed Central PMCID: PMC9112376.

18. Miyabe C, Miyabe Y, Strle K, Kim ND, Stone JH, Luster AD, et al. An expanded population of pathogenic regulatory T cells in giant cell arteritis is abrogated by IL-6 blockade therapy. Ann Rheum Dis. 2017 May 1;76(5):898–905. doi:10.1136/annrheumdis-2016-210070 PubMed PMID: 27927642.

19. Samson M, Greigert H, Ciudad M, Gerard C, Ghesquière T, Trad M, et al. Improvement of Treg immune response after treatment with tocilizumab in giant cell arteritis. Clin Transl Immunol. 2021 Jan 1;10(9):e1332. doi:10.1002/CTI2.1332

20. Weyand CM, Berry GJ, Goronzy JJ. The immunoinhibitory PD-1/PD-L1 pathway in inflammatory blood vessel disease. J Leukoc Biol. 2018 Mar;103(3):565–75. doi:10.1189/jlb.3MA0717-283 PubMed PMID: 28848042; PubMed Central PMCID: PMC6457250.

21. Zhang H, Watanabe R, Berry GJ, Vaglio A, Liao YJ, Warrington KJ, et al. Immunoinhibitory checkpoint deficiency in medium and large vessel vasculitis. Proc Natl Acad Sci U S A. 2017 Feb 7;114(6):E970–9. doi:10.1073/pnas.1616848114 PubMed PMID: 28115719; PubMed Central PMCID: PMC5307483.

22. Daxini A, Cronin K, Sreih AG. Vasculitis associated with immune checkpoint inhibitors-a systematic review. Clin Rheumatol. 2018 Sep;37(9):2579–84. doi:10.1007/s10067-018-4177-0 PubMed PMID: 29923081.

23. Wen Z, Shen Y, Berry G, Shahram F, Li Y, Watanabe R, et al. The microvascular niche instructs T cells in large vessel vasculitis via the VEGF-Jagged 1-Notch pathway. Sci Transl Med. 2017 Jul 19;9(399). doi:10.1126/SCITRANSLMED.AAL3322, PubMed PMID: 28724574.

24. Watanabe R, Maeda T, Zhang H, Berry GJ, Zeisbrich M, Brockett R, et al. MMP (Matrix Metalloprotease)-9-Producing Monocytes Enable T Cells to Invade the Vessel Wall and Cause Vasculitis. Circ Res. 2018 Aug 31;123(6):700–15. doi:10.1161/CIRCRESAHA.118.313206 PubMed PMID: 29970365; PubMed Central PMCID: PMC6202245.

25. Segarra M, Vilardell C, Matsumoto K, Esparza J, Lozano E, Serra-Pages C, et al. Dual function of focal adhesion kinase in regulating integrin-induced MMP-2 and MMP-9 release by human T lymphoid cells. FASEB J Off Publ Fed Am Soc Exp Biol. 2005 Nov;19(13):1875–7. doi:10.1096/fj.04-3574fje PubMed PMID: 16260653.

26. Segarra M, García-Martínez A, Sánchez M, Hernández-Rodríguez J, Lozano E, Grau JM, et al. Gelatinase expression and proteolytic activity in giant-cell arteritis. Ann Rheum Dis. 2007 Nov;66(11):1429–35. doi:10.1136/ard.2006.068148 PubMed PMID: 17502363; PubMed Central PMCID: PMC2111616.

27. Piggott K, Deng J, Warrington K, Younge B, Kubo JT, Desai M, et al. Blocking the NOTCH pathway inhibits vascular inflammation in large-vessel vasculitis. Circulation. 2011 Jan 25;123(3):309–18. doi:10.1161/CIRCULATIONAHA.110.936203 PubMed PMID: 21220737; PubMed Central PMCID: PMC3056570.

28. Wang L, Ai Z, Khoyratty T, Zec K, Eames HL, van Grinsven E, et al. ROS-producing immature neutrophils in giant cell arteritis are linked to vascular pathologies. JCI Insight. 2020 Oct 15;5(20):e139163, 139163. doi:10.1172/jci.insight.139163 PubMed PMID: 32960815; PubMed Central PMCID: PMC7605529.

29. Cid MC, Cebrián M, Font C, Coll-Vinent B, Hernández-Rodríguez J, Esparza J, et al. Cell adhesion molecules in the development of inflammatory infiltrates in giant cell arteritis: inflammation-induced angiogenesis as the preferential site of leukocyte-endothelial cell interactions. Arthritis Rheum. 2000 Jan;43(1):184–94. doi:10.1002/1529-0131(200001)43:1<184::AID-ANR23>3.0.CO;2-N PubMed PMID: 10643715.

30. Maleszewski JJ, Younge BR, Fritzlen JT, Hunder GG, Goronzy JJ, Warrington KJ, et al. Clinical and pathological evolution of giant cell arteritis: a prospective study of follow-up temporal artery biopsies in 40 treated patients. Mod Pathol Off J U S Can

Acad Pathol Inc. 2017 Jun 1;30(6):788–96. doi:10.1038/MODPATHOL.2017.10 PubMed PMID: 28256573.

31. Weyand CM, Goronzy JJ. Medium- and large-vessel vasculitis. N Engl J Med. 2003 Jul 10;349(2):160–9. doi:10.1056/NEJMra022694 PubMed PMID: 12853590.

32. Pryshchep O, Ma-Krupa W, Younge BR, Goronzy JJ, Weyand CM. Vessel-specific Toll-like receptor profiles in human medium and large arteries. Circulation. 2008 Sep 16;118(12):1276–84. doi:10.1161/CIRCULATIONAHA.108.789172 PubMed PMID: 18765390; PubMed Central PMCID: PMC2748975.

33. Kaiser M, Younge B, Björnsson J, Goronzy JJ, Weyand CM. Formation of new vasa vasorum in vasculitis. Production of angiogenic cytokines by multinucleated giant cells. Am J Pathol. 1999 Sep;155(3):765–74. doi:10.1016/S0002-9440(10)65175-9 PubMed PMID: 10487834; PubMed Central PMCID: PMC1866901.

34. Corbera-Bellalta M, Planas-Rigol E, Lozano E, Terrades-García N, Alba MA, Prieto-González S, et al. Blocking interferon γ reduces expression of chemokines CXCL9, CXCL10 and CXCL11 and decreases macrophage infiltration in ex vivo cultured arteries from patients with giant cell arteritis. Ann Rheum Dis. 2016 Jun;75(6):1177–86. doi:10.1136/annrheumdis-2015-208371 PubMed PMID: 26698852.

35. Régnier P, Le Joncour A, Maciejewski-Duval A, Desbois AC, Comarmond C, Rosenzwajg M, et al. Targeting JAK/STAT pathway in Takayasu's arteritis. Ann Rheum Dis. 2020 Jul;79(7):951–9. doi:10.1136/annrheumdis-2019-216900 PubMed PMID: 32213496.

36. Zhang H, Watanabe R, Berry GJ, Tian L, Goronzy JJ, Weyand CM. Inhibition of JAK-STAT Signaling Suppresses Pathogenic Immune Responses in Medium and Large Vessel Vasculitis. Circulation. 2018 May 1;137(18):1934–48. doi:10.1161/CIRCULATIONAHA.117.030423 PubMed PMID: 29254929.

37. Maciejewski-Duval A, Comarmond C, Leroyer A, Zaidan M, Le Joncour A, Desbois AC, et al. mTOR pathway activation in large vessel vasculitis. J Autoimmun. 2018 Nov 1;94:99–109. doi:10.1016/j.jaut.2018.07.013 PubMed PMID: 30061014.

38. Hadjadj J, Canaud G, Mirault T, Samson M, Bruneval P, Régent A, et al. mTOR pathway is activated in endothelial cells from patients with Takayasu arteritis and is modulated by serum immunoglobulin G. Rheumatology. 2018 Jun 1;57(6):1011–20. doi:10.1093/rheumatology/key017 PubMed PMID: 29506143.

39. Soriano A, Muratore F, Pipitone N, Boiardi L, Cimino L, Salvarani C. Visual loss and other cranial ischaemic complications in giant cell arteritis. Nat Rev Rheumatol 2017 138. 2017 Jul 6;13(8):476–84. doi:10.1038/nrrheum.2017.98 PubMed PMID: 28680132.

40. García-Martínez A, Arguis P, Prieto-González S, Espígol-Frigolé G, Alba MA, Butjosa M, et al. Prospective long term follow-up of a cohort of patients with giant cell arteritis screened for aortic structural damage (aneurysm or dilatation). Ann Rheum Dis. 2014 Oct;73(10):1826–32. doi:10.1136/annrheumdis-2013-203322 PubMed PMID: 23873881.

41. Kermani TA, Warrington KJ, Crowson CS, Ytterberg SR, Hunder GG, Gabriel SE, et al. Large-vessel involvement in giant cell arteritis: a population-based cohort study of the incidence-trends and prognosis. Ann Rheum Dis. 2013 Dec;72(12):1989–94. doi:10.1136/annrheumdis-2012-202408 PubMed PMID: 23253927; PubMed Central PMCID: PMC4112513.

42. Pugh D, Karabayas M, Basu N, Cid MC, Goel R, Goodyear CS, et al. Large-vessel vasculitis. Nat Rev Dis Primer. 2022 Dec 1;7(1). doi:10.1038/S41572-021-00327-5 PubMed PMID: 34992251.

43. Parikh M, Miller NR, Lee AG, Savino PJ, Vacarezza MN, Cornblath W, et al. Prevalence of a normal C-reactive protein with an elevated erythrocyte sedimentation rate in biopsy-proven giant cell arteritis. Ophthalmology. 2006 Oct;113(10):1842–5. doi:10.1016/j.ophtha.2006.05.020 PubMed PMID: 16884778.

44. Salvarani C, Cantini F, Boiardi L, Hunder GG. Laboratory investigations useful in giant cell arteritis and Takayasu's arteritis. Clin Exp Rheumatol. 2003;21(6 SUPPL. 32). PubMed PMID: 14740424.

45. Perugino CA, Wallace ZS, Meyersohn N, Oliveira G, Stone JR, Stone JH. Large vessel involvement by IgG4-related disease. Medicine (Baltimore). 2016 Jul;95(28):e3344. doi:10.1097/MD.0000000000003344 PubMed PMID: 27428181.

46. Silvestri V, Simonte G. Aortic Pathology in Systemic Lupus Erythematosus: A Case Report and Review of Literature. Ann Vasc Surg. 2017 Aug;43:312.e5-312.e12. doi:10.1016/j.avsg.2017.01.022 PubMed PMID: 28478171.

47. Monghal V, Puéchal X, Smets P, Vandergheynst F, Michel M, Diot E, et al. Large-vessel involvement in ANCA-associated vasculitis: A multicenter case-control study. Semin Arthritis Rheum. 2024 Aug;67:152475. doi:10.1016/j.semarthrit.2024.152475 PubMed PMID: 38810568.

48. Dejaco C, Ramiro S, Bond M, Bosch P, Ponte C, Mackie SL, et al. EULAR recommendations for the use of imaging in large vessel vasculitis in clinical practice: 2023 update. Ann Rheum Dis. 2024 Jun 1;83(6):741–51. doi:10.1136/ARD-2023-224543 PubMed PMID: 37550004.

49. Schmidt WA, Kraft HE, Vorpahl K, Völker L, Gromnica-Ihle EJ. Color duplex ultrasonography in the diagnosis of temporal arteritis. N Engl J Med. 1997 Nov 6;337(19):1336–42. doi:10.1056/NEJM199711063371902 PubMed PMID: 9358127.

50. Dejaco C, Ponte C, Monti S, Rozza D, Scirè CA, Terslev L, et al. The provisional OMERACT ultrasonography score for giant cell arteritis. Ann Rheum Dis. 2023 Apr 1;82(4):556–64. doi:10.1136/ARD-2022-223367 PubMed PMID: 36600183.

51. Marvisi C, Macaluso F, Ricordi C, Cavazza A, Muratore F, Salvarani C. Diagnostic approach in giant cell arteritis. Autoimmun Rev. 2025 Mar 26;24(4):103743. doi:10.1016/j.autrev.2025.103743 PubMed PMID: 39793744.

52. Muratore F, Boiardi L, Cavazza A, Aldigeri R, Pipitone N, Restuccia G, et al. Correlations between histopathological findings and clinical manifestations in biopsy-proven giant cell arteritis. J Autoimmun. 2016 May 1;69:94–101. doi:10.1016/J.JAUT.2016.03.005 PubMed PMID: 27009904.

53. Habib HM, Essa AA, Hassan AA. Color duplex ultrasonography of temporal arteries: role in diagnosis and follow-up of suspected cases of temporal arteritis. Clin Rheumatol. 2012 Feb;31(2):231–7. doi:10.1007/S10067-011-1808-0 PubMed PMID: 21743987.

54. Karahaliou M, Vaiopoulos G, Papaspyrou S, Kanakis MA, Revenas K, Sfikakis PP. Colour duplex sonography of temporal arteries before decision for biopsy: a prospective study in 55 patients with suspected giant cell arteritis. Arthritis Res Ther. 2006 Jul 19;8(4). doi:10.1186/AR2003 PubMed PMID: 16859533.

55. De Miguel E, Roxo A, Castillo C, Peiteado D, Villalba A, Martín-Mola E. The utility and sensitivity of colour Doppler ultrasound in monitoring changes in giant cell arteritis. Clin Exp Rheumatol. 2012;30(SUPPL. 70). PubMed PMID: 22410311.

56. Hellmich B, Agueda A, Monti S, Buttgereit F, De Boysson H, Brouwer E, et al. 2018 Update of the EULAR recommendations for the management of large vessel vasculitis. Ann Rheum Dis. 2020 Jan 1;79(1):19–130. doi:10.1136/ANNRHEUMDIS-2019-215672 PubMed PMID: 31270110.

57. Maz M, Chung SA, Abril A, Langford CA, Gorelik M, Guyatt G, et al. 2021 American College of Rheumatology/Vasculitis Foundation Guideline for the Management of Giant Cell Arteritis and Takayasu Arteritis. Arthritis Rheumatol Hoboken NJ. 2021 Aug 1;73(8):1349–65. doi:10.1002/ART.41774 PubMed PMID: 34235884.

58. Hunder GG, Bloch DA, Michel BA, Stevens MB, Arend WP, Calabrese LH, et al. The American College of Rheumatology 1990 criteria for the classification of giant cell arteritis. Arthritis Rheum. 1990;33(8):1122–8. doi:10.1002/ART.1780330810 PubMed PMID: 2202311.

59. Slavin ML. Brow Droop After Superficial Temporal Artery Biopsy. Arch Ophthalmol. 1986 Aug 1;104(8):1127–1127. doi:10.1001/ARCHOPHT.1986.01050200033026 PubMed PMID: 3741232.

60. Murchison AP, Bilyk JR. Brow ptosis after temporal artery biopsy: incidence and associations. Ophthalmology. 2012;119(12):2637–42. doi:10.1016/J.OPHTHA.2012.07.020 PubMed PMID: 22986114.

61. Siemssen SJ. On the occurrence of necrotising lesions in arteritis temporalis: review of the literature with a note on the potential risk of a biopsy. Br J Plast Surg. 1987;40(1):73–82. doi:10.1016/0007-1226(87)90015-4 PubMed PMID: 3545346.

62. Rubenstein E, Maldini C, Gonzalez-Chiappe S, Chevret S, Mahr A. Sensitivity of temporal artery biopsy in the diagnosis of giant cell arteritis: a systematic literature review and meta-analysis. Rheumatol Oxf Engl. 2020 May 1;59(5):1011–20. doi:10.1093/RHEUMATOLOGY/KEZ385 PubMed PMID: 31529073.

63. Cavazza A, Muratore F, Boiardi L, Restuccia G, Pipitone N, Pazzola G, et al. Inflamed temporal artery: histologic findings in 354 biopsies, with clinical correlations. Am J Surg Pathol. 2014;38(10):1360–70. doi:10.1097/PAS.0000000000000244 PubMed PMID: 25216320.

64. Luqmani R, Lee E, Singh S, Gillett M, Schmidt WA, Bradburn M, et al. The Role of Ultrasound Compared to Biopsy of Temporal Arteries in the Diagnosis and Treatment of Giant Cell Arteritis (TABUL): a diagnostic accuracy and cost-effectiveness study. Health Technol Assess Winch Engl. 2016;20(90):1–270. doi:10.3310/HTA20900 PubMed PMID: 27925577.

65. Ricordi C, Marvisi C, Macchioni P, Boiardi L, Cavazza A, Croci S, et al. Does tocilizumab eliminate inflammation in GCA? A cohort study on repeated temporal artery biopsies. RMD Open. 2024 Dec 31;10(4):e005132. doi:10.1136/rmdopen-2024-005132 PubMed PMID: 39740930; PubMed Central PMCID: PMC11748933.

66. Schmidt WA, Seifert A, Gromnica-ihle E, Krause A, Natusch A. Ultrasound of proximal upper extremity arteries to increase the diagnostic yield in large-vessel giant cell arteritis. Rheumatol Oxf Engl. 2008 Jan;47(1):96–101. doi:10.1093/RHEUMATOLOGY/KEM322 PubMed PMID: 18077499.

67. Bosch P, Bond M, Dejaco C, Ponte C, Louise Mackie S, Falzon L, et al. Imaging in diagnosis, monitoring and outcome prediction of large vessel vasculitis: a systematic literature review and meta-analysis informing the 2023 update of the EULAR recommendations [Internet]. doi:10.1136/rmdopen-2023-003379

68. Lariviere D, Benali K, Coustet B, Pasi N, Hyafil F, Klein I, et al. Positron emission tomography and computed tomography angiography for the diagnosis of giant cell

arteritis: A real-life prospective study. Medicine (Baltimore). 2016 Jul;95(30):e4146. doi:10.1097/MD.0000000000004146 PubMed PMID: 27472684; PubMed Central PMCID: PMC5265821.

69. Stellingwerff MD, Brouwer E, Lensen KJDF, Rutgers A, Arends S, van der Geest KSM, et al. Different Scoring Methods of FDG PET/CT in Giant Cell Arteritis: Need for Standardization. Medicine (Baltimore). 2015 Sep;94(37):e1542. doi:10.1097/MD.0000000000001542 PubMed PMID: 26376404; PubMed Central PMCID: PMC4635818.

70. Slart RHJA, Writing group, Reviewer group, Members of EANM Cardiovascular, Members of EANM Infection & Inflammation, Members of Committees, SNMMI Cardiovascular, et al. FDG-PET/CT(A) imaging in large vessel vasculitis and polymyalgia rheumatica: joint procedural recommendation of the EANM, SNMMI, and the PET Interest Group (PIG), and endorsed by the ASNC. Eur J Nucl Med Mol Imaging. 2018 Jul;45(7):1250–69. doi:10.1007/s00259-018-3973-8 PubMed PMID: 29637252; PubMed Central PMCID: PMC5954002.

71. Meller J, Strutz F, Siefker U, Scheel A, Sahlmann CO, Lehmann K, et al. Early diagnosis and follow-up of aortitis with [18F]FDG PET and MRI. Eur J Nucl Med Mol Imaging. 2003 May 4;30(5):730–6. doi:10.1007/s00259-003-1144-y

72. Blockmans D, de Ceuninck L, Vanderschueren S, Knockaert D, Mortelmans L, Bobbaers H. Repetitive 18F-fluorodeoxyglucose positron emission tomography in giant cell arteritis: a prospective study of 35 patients. Arthritis Rheum. 2006 Feb 15;55(1):131–7. doi:10.1002/art.21699 PubMed PMID: 16463425.

73. Grayson PC, Alehashemi S, Bagheri AA, Civelek AC, Cupps TR, Kaplan MJ, et al. 18 F-Fluorodeoxyglucose-Positron Emission Tomography As an Imaging Biomarker in a Prospective, Longitudinal Cohort of Patients With Large Vessel Vasculitis. Arthritis Rheumatol Hoboken NJ. 2018 Mar 1;70(3):439–49. doi:10.1002/ART.40379 PubMed PMID: 29145713.

74. Dashora HR, Rosenblum JS, Quinn KA, Alessi H, Novakovich E, Saboury B, et al. Comparing Semiquantitative and Qualitative Methods of Vascular 18F-FDG PET Activity Measurement in Large-Vessel Vasculitis. J Nucl Med Off Publ Soc Nucl Med. 2022 Feb 1;63(2):280–6. doi:10.2967/JNUMED.121.262326 PubMed PMID: 34088771.

75. Nielsen BD, Gormsen LC, Hansen IT, Keller KK, Therkildsen P, Hauge EM. Three days of high-dose glucocorticoid treatment attenuates large-vessel 18F-FDG uptake in large-vessel giant cell arteritis but with a limited impact on diagnostic accuracy. Eur J Nucl Med Mol Imaging. 2018 Jul 1;45(7):1119–28. doi:10.1007/S00259-018-4021-4/METRICS PubMed PMID: 29671039.

76. Einspieler I, Thürmel K, Pyka T, Eiber M, Wolfram S, Moog P, et al. Imaging large vessel vasculitis with fully integrated PET/MRI: a pilot study. Eur J Nucl Med Mol Imaging. 2015 Jun 1;42(7):1012–24. doi:10.1007/S00259-015-3007-8/METRICS PubMed PMID: 25876704.

77. Martin O, Schaarschmidt BM, Kirchner J, Suntharalingam S, Grueneisen J, Demircioglu A, et al. PET/MRI Versus PET/CT for Whole-Body Staging: Results from a Single-Center Observational Study on 1,003 Sequential Examinations. J Nucl Med. 2020 Aug 1;61(8):1131–6. doi:10.2967/JNUMED.119.233940 PubMed PMID: 31806777.

78. van der Geest KSM, Sandovici M, Nienhuis PH, Slart RHJA, Heeringa P, Brouwer E, et al. Novel PET Imaging of Inflammatory Targets and Cells for the Diagnosis and Monitoring of Giant Cell Arteritis and Polymyalgia Rheumatica. Front Med. 2022 Jun 6;9. doi:10.3389/FMED.2022.902155/PDF

79. Ćorović A, Wall C, Nus M, Gopalan D, Huang Y, Imaz M, et al. Somatostatin Receptor PET/MR Imaging of Inflammation in Patients With Large Vessel Vasculitis and Atherosclerosis. J Am Coll Cardiol. 2023 Jan 31;81(4):336–54. doi:10.1016/J.JACC.2022.10.034 PubMed PMID: 36697134.

80. Röhrich M, Rosales JJ, Hoppner J, Kvacskay P, Blank N, Loi L, et al. Fibroblast Activation Protein Inhibitor-Positron Emission Tomography in Aortitis: Fibroblast pathology in active inflammation and remission. Rheumatol Oxf Engl. 2024 Apr 22. doi:10.1093/RHEUMATOLOGY/KEAE225 PubMed PMID: 38648749.

81. Pugliese F, Gaemperli O, Kinderlerer AR, Lamare F, Shalhoub J, Davies AH, et al. Imaging of vascular inflammation with [11C]-PK11195 and positron emission tomography/computed tomography angiography. J Am Coll Cardiol. 2010 Aug 17;56(8):653–61. doi:10.1016/j.jacc.2010.02.063 PubMed PMID: 20705222.

82. Stone JH, Klearman M, Collinson N. Trial of Tocilizumab in Giant-Cell Arteritis. N Engl J Med. 2017 Oct 12;377(15):1494–5. doi:10.1056/NEJMc1711031 PubMed PMID: 29020600.

83. Stone JH, Spotswood H, Unizony SH, Aringer M, Blockmans D, Brouwer E, et al. New-onset versus relapsing giant cell arteritis treated with tocilizumab: 3-year results from a randomized controlled trial and extension. Rheumatology. 2022 Jul 6;61(7):2915–22. doi:10.1093/RHEUMATOLOGY/KEAB780 PubMed PMID: 34718434.

84. Blockmans D, Penn SK, Setty AR, Schmidt WA, Rubbert-Roth A, Hauge EM, et al. A Phase 3 Trial of Upadacitinib for Giant-Cell Arteritis. N Engl J Med. 2025 May 29;392(20):2013–24. doi:10.1056/NEJMoa2413449 PubMed PMID: 40174237.

85. Investigators G, Han J, Bao M, Stone JH, Han J, Aringer M, et al. Long-term effect of tocilizumab in patients with giant cell arteritis Long-term effect of tocilizumab in patients with giant cell arteritis: open-label extension phase of the Giant Cell Arteritis Actemra (GiACTA) trial for the GiACTA investigators* [Internet]. 2021. doi:10.1016/S2665-9913(21)00038-2

86. Christ L, Seitz L, Scholz G, Sarbu AC, Amsler J, Bütikofer L, et al. Tocilizumab monotherapy after ultra-short glucocorticoid administration in giant cell arteritis: a single-arm, open-label, proof-of-concept study. Lancet Rheumatol. 2021 Sep 1;3(9):e619–26. doi:10.1016/S2665-9913(21)00152-1

87. Muratore F, Marvisi C, Cassone G, Boiardi L, Mancuso P, Besutti G, et al. Treatment of giant cell arteritis with ultra-short glucocorticoids and tocilizumab: the role of imaging in a prospective observational study. Rheumatol Oxf Engl. 2024 Jan 4;63(1). doi:10.1093/RHEUMATOLOGY/KEAD215 PubMed PMID: 37195423.

88. Evans JM, O'Fallon WM, Hunder GG. Increased incidence of aortic aneurysm and dissection in giant cell (temporal) arteritis. A population-based study. Ann Intern Med. 1995 Apr 1;122(7):502–7. doi:10.7326/0003-4819-122-7-199504010-00004 PubMed PMID: 7872584.

89. Robson JC, Kiran A, Maskell J, Hutchings A, Arden N, Dasgupta B, et al. The relative risk of aortic aneurysm in patients with giant cell arteritis compared with the general population of the UK. Ann Rheum Dis. 2015 Jan;74(1):129–35. doi:10.1136/annrheumdis-2013-204113 PubMed PMID: 24095936.

90. Therkildsen P, de Thurah A, Nielsen BD, Hansen IT, Eldrup N, Nørgaard M, et al. Increased risk of thoracic aortic complications among patients with giant cell arteritis: a nationwide, population-based cohort study. Rheumatology. 2022 Jul 6;61(7):2931–41. doi:10.1093/rheumatology/keab871 PubMed PMID: 34918058.

91. Mackie SL, Hensor EMA, Morgan AW, Pease CT. Should I send my patient with previous giant cell arteritis for imaging of the thoracic aorta? A systematic literature review and meta-analysis. Ann Rheum Dis. 2014 Jan;73(1):143–8. doi:10.1136/annrheumdis-2012-202145 PubMed PMID: 23264356.

92. Kaymakci MS, Boire NA, Bois MC, Elfishawi MM, Langenfeld HE, Hanson AC, et al. Persistent aortic inflammation in patients with giant cell arteritis. Autoimmun Rev. 2023 Sep;22(9):103411. doi:10.1016/j.autrev.2023.103411 PubMed PMID: 37597603; PubMed Central PMCID: PMC10528001.

93. Soussan M, Nicolas P, Schramm C, Katsahian S, Pop G, Fain O, et al. Management of large-vessel vasculitis with FDG-PET: a systematic literature review and meta-analysis. Medicine (Baltimore). 2015 Apr 6;94(14). doi:10.1097/MD.0000000000000622 PubMed PMID: 25860208.

94. Galli E, Muratore F, Mancuso P, Boiardi L, Marvisi C, Besutti G, et al. The role of PET/CT in disease activity assessment in patients with large vessel vasculitis. Rheumatol Oxf Engl. 2022 Mar 8. doi:10.1093/RHEUMATOLOGY/KEAC125 PubMed PMID: 35258570.

95. van der Geest KSM, Treglia G, Glaudemans AWJM, Brouwer E, Sandovici M, Jamar F, et al. Diagnostic value of [18F]FDG-PET/CT for treatment monitoring in large vessel vasculitis: a systematic review and meta-analysis. Eur J Nucl Med Mol Imaging. 2021 Nov 1;48(12):3886. doi:10.1007/S00259-021-05362-8 PubMed PMID: 33942141.

96. Prieto-González S, Arguis P, García-Martínez A, Espígol-Frigolé G, Tavera-Bahillo I, Butjosa M, et al. Large vessel involvement in biopsy-proven giant cell arteritis: prospective study in 40 newly diagnosed patients using CT angiography. Ann Rheum Dis. 2012 Jul;71(7):1170–6. doi:10.1136/ANNRHEUMDIS-2011-200865 PubMed PMID: 22267328.

97. Writing Committee Members, Isselbacher EM, Preventza O, Hamilton Black Iii J, Augoustides JG, Beck AW, et al. 2022 ACC/AHA Guideline for the Diagnosis and Management of Aortic Disease: A Report of the American Heart Association/American College of Cardiology Joint Committee on Clinical Practice Guidelines. J Am Coll Cardiol. 2022 Dec 13;80(24):e223–393. doi:10.1016/j.jacc.2022.08.004 PubMed PMID: 36334952; PubMed Central PMCID: PMC9860464.

98. Muratore F, Marvisi C, Cassone G, Ricordi C, Boiardi L, Mancuso P, et al. Treatment of giant cell arteritis with ultra-short glucocorticoids and tocilizumab: results from the extension of the TOPAZIO study. Rheumatology. 2025 May 1;64(5):3057–62. doi:10.1093/rheumatology/keae400 PubMed PMID: 39150490.

99. García-Martínez A, Hernández-Rodríguez J, Arguis P, Paredes P, Segarra M, Lozano E, et al. Development of aortic aneurysm/dilatation during the followup of patients with giant cell arteritis: a cross-sectional screening of fifty-four prospectively followed patients. Arthritis Rheum. 2008 Mar 15;59(3):422–30. doi:10.1002/art.23315 PubMed PMID: 18311764.

100. García-Martínez A, Arguis P, Prieto-González S, Espígol-Frigolé G, Alba MA, Butjosa M, et al. Prospective long term follow-up of a cohort of patients with giant cell arteritis screened for aortic structural damage (aneurysm or dilatation). Ann Rheum Dis. 2014 Oct;73(10):1826–32. doi:10.1136/annrheumdis-2013-203322 PubMed PMID: 23873881.

101. Agard C, Barrier JH, Dupas B, Ponge T, Mahr A, Fradet G, et al. Aortic involvement in recent-onset giant cell (temporal) arteritis: a case-control prospective study using helical aortic computed tomodensitometric scan. Arthritis Rheum. 2008 May 15;59(5):670–6. doi:10.1002/art.23577 PubMed PMID: 18438900.

102. Muratore F, Crescentini F, Spaggiari L, Pazzola G, Casali M, Boiardi L, et al. Aortic dilatation in patients with large vessel vasculitis: A longitudinal case control study using PET/CT. Semin Arthritis Rheum. 2019 Jun;48(6):1074–82. doi:10.1016/j.semarthrit.2018.10.003 PubMed PMID: 30424972.

103. de Boysson H, Daumas A, Vautier M, Parienti JJ, Liozon E, Lambert M, et al. Large-vessel involvement and aortic dilation in giant-cell arteritis. A multicenter study of 549 patients. Autoimmun Rev. 2018 Apr;17(4):391–8. doi:10.1016/j.autrev.2017.11.029 PubMed PMID: 29427822.

104. de Boysson H, Liozon E, Lambert M, Parienti JJ, Artigues N, Geffray L, et al. 18F-fluorodeoxyglucose positron emission tomography and the risk of subsequent aortic complications in giant-cell arteritis: A multicenter cohort of 130 patients. Medicine (Baltimore). 2016 Jun;95(26):e3851. doi:10.1097/MD.0000000000003851 PubMed PMID: 27367985; PubMed Central PMCID: PMC4937899.

105. Blockmans D, Moreel L, Betrains A, Vanderschueren S, Coudyzer W, Boeckxstaens L, et al. Association between vascular FDG uptake during follow-up and the development of thoracic aortic aneurysms in giant cell arteritis. Front Med. 2024;11. doi:10.3389/FMED.2024.1384533/PDF

106. Moreel L, Coudyzer W, Boeckxstaens L, Betrains A, Molenberghs G, Vanderschueren S, et al. Association Between Vascular 18F-Fluorodeoxyglucose Uptake at Diagnosis and Change in Aortic Dimensions in Giant Cell Arteritis : A Cohort Study. Ann Intern Med. 2023 Oct;176(10):1321–9. doi:10.7326/M23-0679 PubMed PMID: 37782924.

107. Guerra L, Chauvie S, Fallanca F, Bergesio F, Marcheselli L, Durmo R, et al. End of induction [18F]FDG PET is prognostic for progression-free survival and overall survival in follicular lymphoma patients enrolled in the FOLL12 trial. Eur J Nucl Med Mol Imaging. 2024 Sep;51(11):3311–21. doi:10.1007/s00259-024-06765-z PubMed PMID: 38795120.

108. Boellaard R, Buvat I, Nioche C, Ceriani L, Cottereau AS, Guerra L, et al. International Benchmark for Total Metabolic Tumor Volume Measurement in Baseline 18F-FDG PET/CT of Lymphoma Patients: A Milestone Toward Clinical Implementation. J Nucl Med Off Publ Soc Nucl Med. 2024 Sep 3;65(9):1343–8. doi:10.2967/jnumed.124.267789 PubMed PMID: 39089812; PubMed Central PMCID: PMC11372260.

109. Hemmig AK, Aschwanden M, Berger CT, Kyburz D, Mensch N, Staub D, et al. Prior polymyalgia rheumatica is associated with sonographic vasculitic changes in newly diagnosed patients with giant cell arteritis. Rheumatology. 2024 May 3;63(6):1523–7. doi:10.1093/rheumatology/kead450 PubMed PMID: 37647653; PubMed Central PMCID: PMC11147534.

110. Cowley S, Harkins P, Kirby C, Conway R, Kane D. Real-world outcomes of a dedicated fast-track polymyalgia rheumatica clinic. Rheumatology. 2025 May 1;64(5):3006–11. doi:10.1093/rheumatology/keae531 PubMed PMID: 39348187; PubMed Central PMCID: PMC12048043.

111. De Miguel E, Macchioni P, Conticini E, Campochiaro C, Karalilova R, Monti S, et al. Prevalence and characteristics of subclinical giant cell arteritis in polymyalgia rheumatica. Rheumatology. 2024 Jan 4;63(1):158–64. doi:10.1093/rheumatology/kead189 PubMed PMID: 37129541.

112. De Miguel E, Karalilova R, Macchioni P, Ponte C, Conticini E, Cowley S, et al. Subclinical giant cell arteritis increases the risk of relapse in polymyalgia rheumatica. Ann Rheum Dis. 2024 Feb 15;83(3):335–41. doi:10.1136/ard-2023-224768 PubMed PMID: 37932008.

113. Kaymakci MS, Berry GJ, Langenfeld HE, Hanson AC, Crowson CS, Bois MC, et al. Subclinical aortic inflammation in patients with polymyalgia rheumatica. Rheumatology. 2024 Dec 1;63(12):3289–96. doi:10.1093/rheumatology/keae373 PubMed PMID: 39024049; PubMed Central PMCID: PMC11637548.

114. van der Geest KSM, Sandovici M, Bley TA, Stone JR, Slart RHJA, Brouwer E. Large vessel giant cell arteritis. Lancet Rheumatol. 2024 Jun;6(6):e397–408. doi:10.1016/S2665-9913(23)00300-4 PubMed PMID: 38574745.

115. Tomelleri A, Campochiaro C, Sartorelli S, Farina N, Baldissera E, Dagna L. Presenting features and outcomes of cranial-limited and large-vessel giant cell arteritis: a retrospective cohort study. Scand J Rheumatol. 2022 Jan;51(1):59–66. doi:10.1080/03009742.2021.1889025 PubMed PMID: 33913792.

116. Ora M, Misra DP, Kavadichanda CG, Singh K, Rathore U, Jain N, et al. Metabolic inflammatory volume and total inflammatory glycolysis: novel parameters to evaluate PET-CT disease activity in Takayasu arteritis. Clin Rheumatol. 2023 Jul;42(7):1855–61. doi:10.1007/s10067-023-06600-0 PubMed PMID: 37055597.

117. van der Geest KSM, Gheysens O, Gormsen LC, Glaudemans AWJM, Tsoumpas C, Brouwer E, et al. Advances in PET Imaging of Large Vessel Vasculitis: An Update and Future Trends. Semin Nucl Med. 2024 Sep;54(5):753–60. doi:10.1053/j.semnuclmed.2024.03.001 PubMed PMID: 38538456.